MICROCOPY RESOLUTION TEST CHART
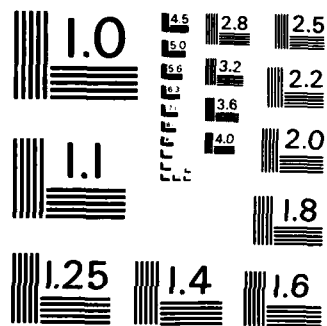
NATIONAL BUREAU OF STANDARDS-1963-A

E801223

②

AFATL-TR-85-65

AD-A161 825

Conceptual Design and Analysis of High Speed Electronic Imaging-Phase I
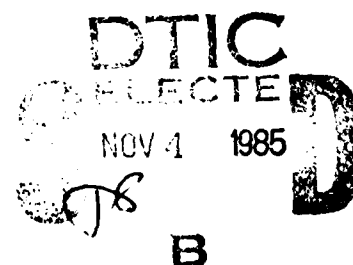
RANDY BROWN
J R PARKER

LOS ALAMOS NATIONAL LABORATORY
GROUP E-8, MS E523
LOS ALAMOS, NEW MEXICO 87545

OCTOBER 1985

DTIC
ELECTE
NOV 4 1985

B

FINAL REPORT FOR PERIOD NOVEMBER 1982—SEPTEMBER 1984
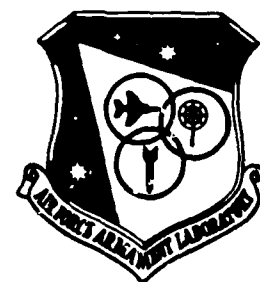
DTIC FILE COPY

Air Force Armament Laboratory

AIR FORCE SYSTEMS COMMAND ★ UNITED STATES AIR FORCE ★ EGLIN AIR FORCE BASE, FLORIDA

85 11 04 060

NOTICE

When Government drawings, specifications, or other data are used for any purpose other than in connection with a definitely related Government procurement operation, the United States Government thereby incurs no responsibility nor any obligation whatsoever; and the fact that the Government may have formulated, furnished, or in any way supplied the said drawings, specifications, or other data, is not to be regarded by implication or otherwise as in any manner licensing the holder or any other person or corporation, or conveying any rights or permission to manufacture, use, or sell any patented invention that may in any way be related thereto.

This report has been reviewed by the Public Affairs Office (PA) and is releasable to the National Technical Information Service (NTIS). At NTIS, it will be available to the general public, including foreign nations.

This technical report has been reviewed and is approved for publication.

FOR THE COMMANDER

DONALD C. DANIEL
Chief, Aeromechanics Division

Even though this report may contain special release rights held by the controlling office, please do not request copies from the Air Force Armament Laboratory. If you qualify as a recipient, release approval will be obtained from the originating activity by DTIC. Address your request for additional copies to:

> Defense Technical Information Center
> Cameron Station
> Alexandria, Virginia 22314

If your address has changed, if you wish to be removed from our mailing list, or if the addressee is no longer employed by your organization, please notify AFATL/DLCA, Eglin AFB FL 32542.

Copies of this report should not be returned unless return is required by security considerations, contractual obligations, or notice on a specific document.

REPORT DOCUMENTATION PAGE

1a. REPORT SECURITY CLASSIFICATION	1b. RESTRICTIVE MARKINGS
Unclassified	

2a. SECURITY CLASSIFICATION AUTHORITY	3. DISTRIBUTION/AVAILABILITY OF REPORT
	Approved for public release; distribution is unlimited.
2b. DECLASSIFICATION/DOWNGRADING SCHEDULE	

4. PERFORMING ORGANIZATION REPORT NUMBER(S)	5. MONITORING ORGANIZATION REPORT NUMBER(S)
LA-10072-MS	AFATL-TR-85-65

6a. NAME OF PERFORMING ORGANIZATION	6b. OFFICE SYMBOL (If applicable)	7a. NAME OF MONITORING ORGANIZATION
Los Alamos National Labs	N/A	AFATL/DLCA

6c. ADDRESS (City, State and ZIP Code)	7b. ADDRESS (City, State and ZIP Code)
Grp E-8, MS E523, Los Alamos Nat'l Labs Los Alamos, NM 87545	Eglin AFB FL 32542-5000

8a. NAME OF FUNDING/SPONSORING ORGANIZATION	8b. OFFICE SYMBOL (If applicable)	9. PROCUREMENT INSTRUMENT IDENTIFICATION NUMBER
Air Force Armament Lab	AFATL/DLCA	MIPR FY7621-83-90003

8c. ADDRESS (City, State and ZIP Code)	10. SOURCE OF FUNDING NOS.			
AFATL/DLCA Eglin AFB FL 32542-5000	PROGRAM ELEMENT NO.	PROJECT NO.	TASK NO.	WORK UNIT NO.
	62602F	2567	07	25

11 TITLE (Include Security Classification)
Conceptual Design and Analysis of High Speed Electronic Imaging-Phase I

12. PERSONAL AUTHOR(S)
Randy Brown and J.R. Parker

13a. TYPE OF REPORT	13b. TIME COVERED	14. DATE OF REPORT (Yr., Mo., Day)	15. PAGE COUNT
Final	FROM Nov 82 TO Sep 84	1985 October	47

16. SUPPLEMENTARY NOTATION

17.	COSATI CODES		18. SUBJECT TERMS (Continue on reverse if necessary and identify by block number)
FIELD	GROUP	SUB. GR.	Conceptual Design and Analysis of High Speed Electronic Imaging-Phase I
1402	0101	2006	

19 ABSTRACT (Continue on reverse if necessary and identify by block number)

This study addresses the feasibility of using electronic imaging technology for aeroballistics research. Electronic imaging devices are analyzed with respect to range system characteristics. Optical imaging and illumination parameters in the existing system are defined and quantified. System imaging capability is measured and described by modern imaging systems analysis in terms of the system response to a step function input. Two independent measurements that determine system illumination are described and supporting analysis is included.

Concepts critical to data analysis are discussed, along with a survey of available hardware that will image and process projectile flight path data. Recommendations pertinent to the selection of hardware and the overall system organization and maintenance are made.

20 DISTRIBUTION/AVAILABILITY OF ABSTRACT	21. ABSTRACT SECURITY CLASSIFICATION
UNCLASSIFIED/UNLIMITED ☐ SAME AS RPT ☒ DTIC USERS ☐	Unclassified

22a. NAME OF RESPONSIBLE INDIVIDUAL	22b TELEPHONE NUMBER (Include Area Code)	22c. OFFICE SYMBOL
R. J. KELLEY	(904) 882-4086	AFATL/DLCA

DD FORM 1473, 83 APR EDITION OF 1 JAN 73 IS OBSOLETE.

PREFACE

This program was conducted by the Los Alamos National Laboratory, Los Alamos, NM 87545, under a Memorandum of Agreement (MIPR FY7621-83-90003) with the Air Force Armament Laboratory, Armament Division, Eglin Air Force Base, FL 32542. Mr. R.J. Kelley, DLCA, managed the program for the Armament Laboratory. The program was conducted during the period from Sept 1982 to Sept 1984.

Dist.

A-1

i

(The reverse of this page is blank)

TABLE OF CONTENTS

LIST OF FIGURES

LIST OF TABLES

SECTION I

INTRODUCTION

The Eglin Aeroballistics range is an enclosed structure for recording projectile flight paths, Reference 1. The projectiles are in various shapes and may travel at speeds up to MACH 6. They are imaged at regular intervals along the flight path so that an aerodynamic analysis can be conducted. At each recording station, orthogonal image pairs are collected. Each station is out-fitted with two 4 by 5 cameras as shown in Figure 1. Various support electronics accompanying the camera provide shutter control and time-recording functions.

The projectile is illuminated by a Hi-Voltage model SS55P spark-gap flash positioned adjacent to each camera. The flash duration is approximately 0.3 μs. The flash can be considered a point source of light; therefore, the projectile casts a well-defined shadow on the special reflective surface (3M No. 7610) on the opposite wall. The flash is activated at a predetermined time after the projectile passes an infrared linear array positioned near the camera.

Our task is to investigate replacing the existing film cameras with electronic imaging (EI) devices to reduce the delays and the labor-intensive operation associated with the present facility. The conceptual design requires that the resolution of the existing system be maintained and the cameras be replaced without perturbing the rest of the system.
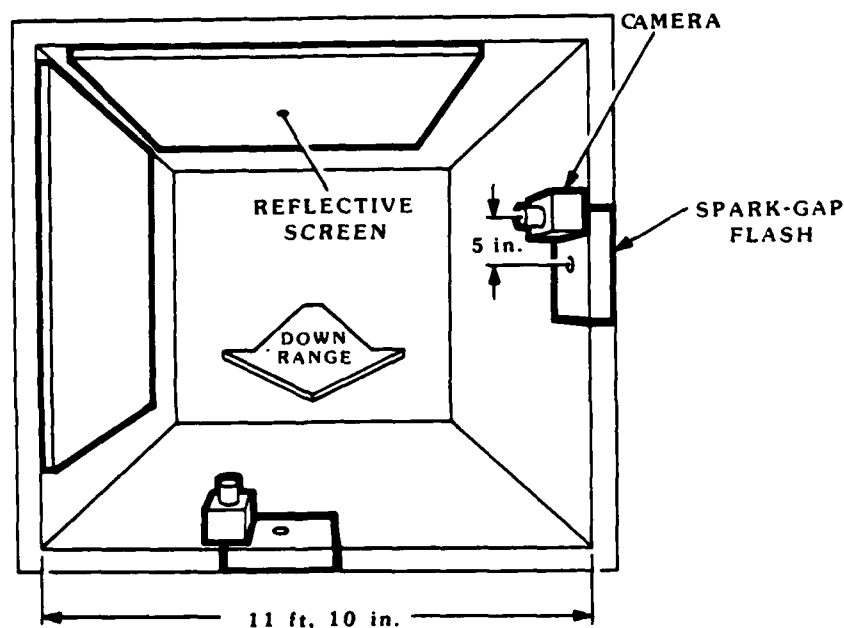

Figure 1. Typical Shadowgraph Station

1

SECTION II
ANALYSIS OF FACILITY

Physical and temporal restrictions imposed by modern aeroballistics have pushed imaging technology to the point where special photoconductive surfaces and high-speed support electronics are dictated. Specifications for these devices can be formulated by a methodical analysis of critical parameters and their interaction. In terms of system theory, system transfer functions and state equations can be used in optimal coupling of devices to maximize system performance. Application of these methods to EI at Eglin is described in this report.

The EI system must autonomously collect and permanently archive an image. It must provide capabilities equivalent to existing hardware, Reference 2; performance has been defined relative to the existing equipment. The EI system must be capable of acquiring an image in 0.3 µs. An air-gap flash will illuminate the object field with sensor spectral optimization provided for low light requirements. The system resolution must be consistent with the existing equipment.

From the onset, it was clear that a spatial, temporal, and spectral characterization of the system was needed to accurately specify EI hardware; more fundamentally, such a characterization was needed to determine if the project was realizable with current state-of-the-art devices. Therefore, theoretical analysis of the system was done to justify the underlying principles of the proposed EI system. The analysis resulted in a favorable outlook for the proposed system. The next step was to analyze the system by means of empirical data. This analysis consisted of two primary determinations: the system transfer function; and, the spectral output of the light source.

First, system resolution was defined in terms of signal-to-noise (S/N) ratio, as compatible with commercial sensor data. Second, spectral response of the system was quantified, which was necessary for optimizing the spectral sensitivity of the EI sensor to the existing light source. These two steps are covered in this section.

Theoretical analysis established initial problems and concepts in EI. General digital EI resolution limitations were evaluated along with image processing techniques for a posteriori error correction. In addition, the study in Sec. II.6. established inherent limitations in both Kodak Royal X-Pan film and EI devices.

2

1. IMAGE ACQUISITION

The images to be analyzed are two-dimensional projections of fast
changing three-dimensional systems. Therefore, we needed an accurate time
history of a projectile in flight in three dimensions. Recording orthogonal
projections at various sample times during the flight provided this accurate
history. Complete three-dimensional information pertaining to the attitude of
the projectile can be obtained if the projections are orthogonal to each other
and if the imaging system has sufficient resolution.

A digital image is a discrete representation of a continuous real image.
Enough samples of a continuous image must be taken to preserve the fine detail
(or resolution). Field-of-view and resolution concepts must be examined to
determine minimal specifications of the imaging system. A field of view is
normally an image that consists of an array of numerical points (N_p x N_p).
The field of view must be large enough to contain the projectile each time it
is fired, since it is uncertain where the projectile will be in the field of
view. Enlarging the field of view without adding more points (that is, making
N_p larger) lessens the detail that can be measured in the vicinity of the
projectile; therefore, it is desirable that the projectile image fill up the
field of view as much as possible.

With the field-of-view and resolution relationships known, the amount of
fine detail in the projectile image to be preserved must be specified. Using
the two-dimensional Nyquist sampling criteria that require sampling at spatial
frequency twice that of the finest detail satisfies this requirement. If
spatial sampling frequency is not high enough, two-dimensional aliasing will
produce artifacts and moiré effects in a reconstructed image.

Only careful examination of all parameters in an imaging system and of
the results desired can dictate the actual specifications to be built into any
imaging system. However, certain crude estimates of imaging system perform-
ance can be made for a set of assumptions that pertain to the system. Con-
sider a projectile image whose long axis fills up fraction $\underline{f}$ of the field of
view of an N_p x N_p image. Further, assume that the projectile image is
sampled at the two-dimensional Nyquist spatial frequency. Then geometric
considerations alone, given uncertainties in the location of the end points of
the long axis, will introduce a minimum error associated with any measure-
ment. Any angle, measured for the long axis, can be in error by $\pm\beta$, where

3

$$\beta = \tan^{-1}\left(\frac{2}{f N_p - 2}\right) .$$

Other errors in measurement, such as improper Nyquist rate, will add to this minimum error. The relationship between image accuracy and variation of N_p and $\underline{f}$ is clearly shown in Table I.

TABLE 1.   LONG-AXIS ANGLE MEASUREMENT ERROR
(β degrees)

$\underline{f}$	N_p			
	1000	500	250	100
0.05	2.4	5.0	11.0	34.0
0.10	1.2	2.4	5.0	14.0
0.25	0.46	0.93	1.9	5.0
0.50	0.23	0.46	0.93	2.4

2.   A POSTERIORI IMAGE PROCESSING

Image processing is the manipulation, usually by digital computer, of the acquired image with intent to detect or enhance some feature. For a projectile, image processing should dynamically measure the attitude of the model in two orthogonal projection planes. Various image processing operations, such as edge detection and smoothing to eliminate moire effects, will be required.

a. Correcting System Distortion and Noise. Camera lenses commonly exhibit nonlinear distortion both in the radial distance from the lens mid-point axis and in the distance of the object from the image plane, Figure 2.

In addition, the detector can distort the image by nature of the physical recording process and add noise because of digitization. Characterizing the lens and the detector mathematically can remove the distortion effects to significantly improve image resolution.

b. Matnematical Model. Each component of the camera system affects the resulting image and can be treated separately. The camera lens and the television sensor or array detector act on the image-forming light, Figure 3. In addition to the effect of the detector on the image, the sensors s{b} may have a signal-dependent noise effect n_3 on the image.
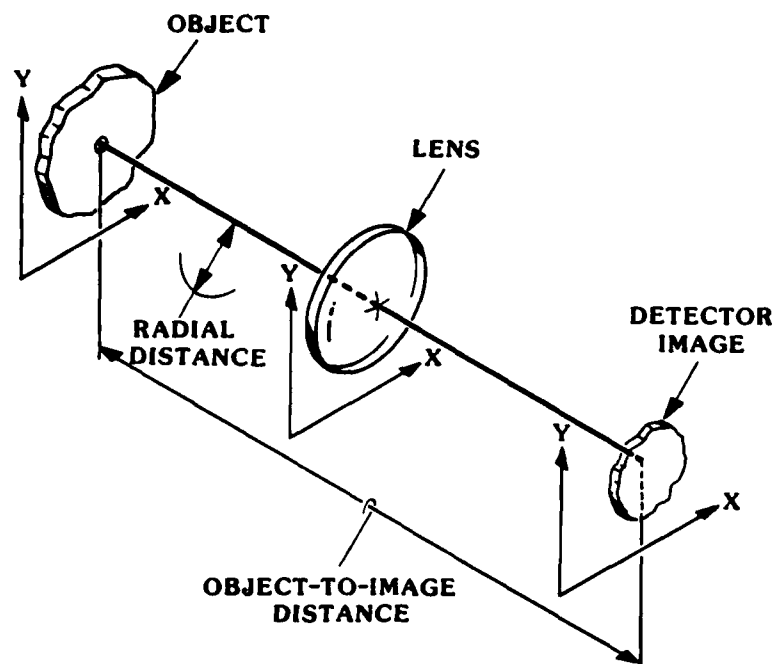
Figure 2.   Image Geometry Model
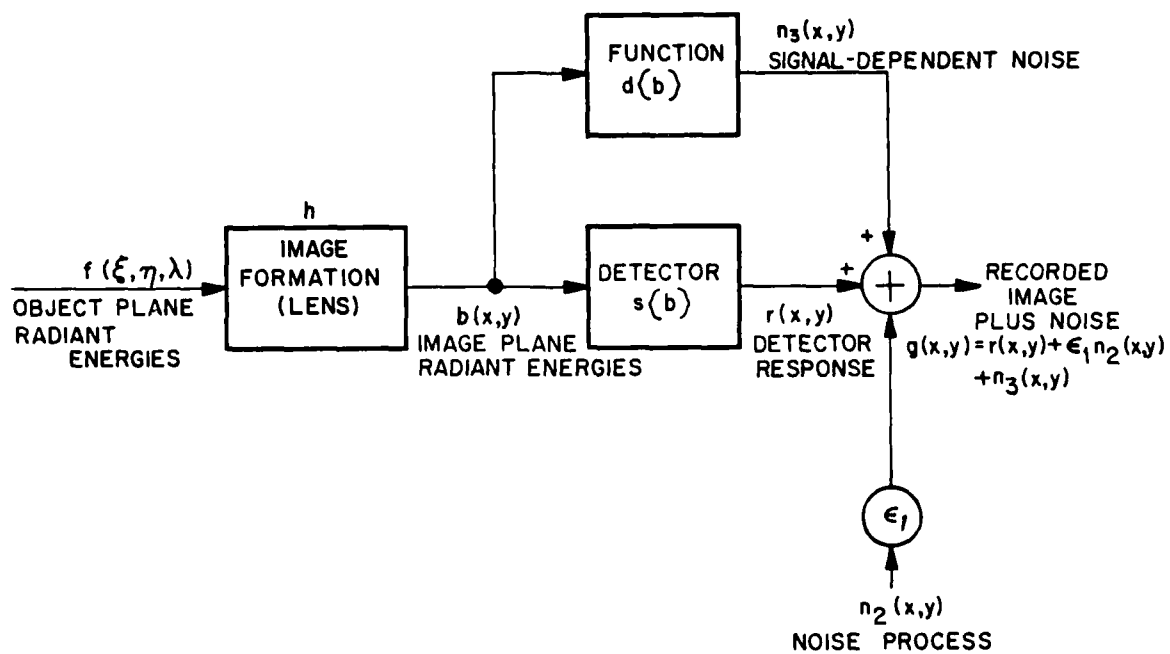
Figure 3.   Transfer Function Model of the Imaging Process

5

Quantization and electrical noises are added noise sources n_2 that also affect the image.

   c. Image Reconstruction. The recorded imag· from a camera is an array of N^2 data entries. Using the lens point-spread-function matrix,* we can represent the lens output in state space as

$$\bar{g} = [H]\bar{f} \quad,$$

where $\bar{g}$ is the image plane matrix with N by N elements contiguously arranged into a vector and $\bar{f}$ is the N by N matrix digital representation of the object plane contiguously arranged into a vector. H is the frequency domain transfer function, and its dimensions are the square of the number of elements in the image plane (in practice many of the elements will be zero or contain no information). The transfer function-in-state space of the entire system (Figure 3) is

$$\bar{g} = s\{[H]\bar{f}\} + d\{[H]\bar{f}\} + \bar{n}_2 \quad.$$

Now the image $\bar{f}'$ can be restored by the nonlinear operator T.

$$\bar{f}' = T[\bar{g}] = T\{s([H]\bar{f}) + d([H]\bar{f}) + \bar{n}_2\} \quad.$$

Fortunately, television cameras are equipped with corrector circuits to cancel signal-dependent noise produced by the sensors; therefore,

$$\bar{f}' = T\{s([H]\bar{f}) + \bar{n}_2\} \quad.$$

Then the natural choice for the restoration process is

$$T = [H]^{-1}s^{-1} \quad;$$

---

*The lens point-spread-function matrix can be obtained at Los Alamos facilities or from commercial optics laboratories.

therefore,

$$\bar{f}' = [H]^{-1}s^{-1}\{s([H]f) + \bar{n}_2\} , \quad \text{and}$$

$$\bar{f}' = \bar{f} + [H]^{-1}s^{-1}\bar{n}_2 .$$

The result is a restored image $\bar{f}'$ exactly like the original object plus the noise acted on by the inverse detector and lens point-spread functions. The noise is nominally small thereby reducing the significance of this term.

The camera lens may significantly distort the object relative to the distance from the image plane. We can use the above equations to correct this distortion, but we must know the projectile size and object-to-image scale factor to calculate the distance from the actual image. The scale factor would be a constant determined when the camera was installed. Projectile size would be an input parameter fed to the computer, and the image plane size would be calculated by the computer.

d. Projectile Position. The exact position of the projectile tip is difficult to determine directly because of the finite number of points that make up the projectile image when the dominant spectral content of the shape of the projectile tip exceeds the Nyquist frequency limit. The Nyquist frequency limit can be calculated from the general expression of uniform grid sampling, and then an expression can be derived for the minimum radius of curvature. Note that the dimension units for frequency are radians per distance using the grid sampling technique (Figure 4):

$$g_s(m\Delta x, n\Delta y) = \sum_m^{\infty} \sum_n^{\infty} g(x,y) \, \delta(x - m\Delta x, y - n\Delta y) ,$$

where δ is the Dirac delta function. The Fourier transform of the image is (ω = radians per distance, $i = -1$)

$$G(\omega_x, \omega_y) = \int_{-\infty}^{\infty} \int_{-\infty}^{\infty} g(x,y) \, \exp\left[-2\pi i(\omega_x x + \omega_y y)\right] \, dx \, dy .$$

7
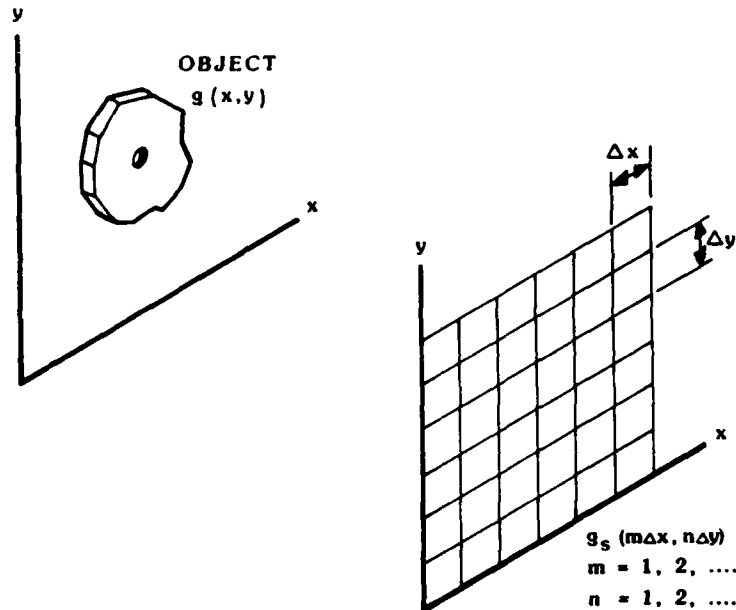
Figure 4. Uniform Grid Sampling

For an infinite Dirac delta field, the Fourier transform is

$$S(\omega_x, \omega_y) = \int_{-\infty}^{\infty} \int_{-\infty}^{\infty} \sum_m^{\infty} \sum_n^{\infty} \delta(x - m\Delta x, y - m\Delta y) \exp\left[-2\pi i(\omega_x x + \omega_y y)\right] dx\ dy$$

$$= \frac{4\pi^2}{\Delta x\ \Delta y} \sum_m^{\infty} \sum_n^{\infty} \delta\ \omega_x - \left(\frac{2\pi m}{\Delta x},\ \omega_y - \frac{2\pi n}{\Delta y}\right)\ .$$

Convolving the two to get a sampled image yields

$$G_s(\omega_x, \omega_y) = G(\omega_x, \omega_y) \star S(\omega_x, \omega_y)$$

$$= \frac{4\pi^2}{\Delta x\ \Delta y} \sum_m^{\infty} \sum_n^{\infty} G\left(\omega_x - \frac{2\pi m}{\Delta x},\ \omega_y - \frac{2\pi n}{\Delta y}\right)\ .$$

8

The Nyquist frequency limit is then

$$\omega_{xc} = \frac{2\pi}{2\,\Delta x} \quad \text{and} \quad \omega_{yc} = \frac{2\pi}{2\,\Delta y} \quad \text{or}$$

$$\omega_{xc} = \frac{\pi}{\Delta x} \quad \text{and} \quad \omega_{yc} = \frac{\pi}{\Delta y} \ .$$

When we approximate the radius of curvature as one-fourth cycle,

$$\frac{2\pi}{4\omega_{xc}} = \frac{2\pi}{4\pi/\Delta x} = \frac{\Delta x}{2} \ .$$

Minimum radius of curvature is then

$$r_{xmin} = \frac{\Delta x}{2} \quad \text{and}$$

$$r_{ymin} = \frac{\Delta y}{2} \ .$$

For projectile tips with a radius of curvature less than r_{min}, the tip position must be approximated. The tip could be generated from statistically selected points on the projectile perimeter using standard predictive estimation routines.

3. SYSTEM TRANSFER FUNCTION

The system transfer function was acquired by using empirical data. In this way the effects of the lens system, film medium, developing process, and illumination source are encompassed in a single format from which a definitive answer to system resolution can be drawn.

The basic data set required is the time domain impulse response f(t) of the system. From this the Fourier transform, Equation (1) can be applied to get the transfer function F(x); that is,

$$F(x) = \mathcal{F}[f(t)] = \int_{-\infty}^{\infty} f(t)\exp[-j2\pi tx]dt \ . \tag{1}$$

9

This method requires use of an impulse as the system input. Because this is a physically unrealizable entity, a step function was used. The step was produced on precision-ground glass using special in-house photograph-masking equipment. A step function S(t) can be related to an impulse function $\delta(t)$ by Equation (2).

$$\delta(t) = \frac{dS(t)}{dt} \; .$$

(2)

Once the Fourier transform of the step response has been calculated, the transfer function may be derived by relating Equation (2) to Fourier space. Given that

$$f(x) \xrightarrow{\mathcal{F}} F(t) \; ,$$

the inverse Fourier transform is

$$f(t) = \int_{-\infty}^{\infty} F(x)\exp(j2\pi xt)dx \; .$$

(3)

Differentiating both sides gives

$$\frac{df(t)}{dt} = \frac{d}{dt}\int_{-\infty}^{\infty} F(x)\exp(j2\pi xt)dx$$

$$= \int_{-\infty}^{\infty} (j2\pi x)\, F(x)\exp(j2\pi xt)dx \; ,$$

(4)

and comparing Equation (4) with Equation (3) clearly shows that $[df(t)]/dt$ and $(j2\pi x)\, F(x)$ are a Fourier transform pair. Thus, the transfer function is obtained by dividing the Fourier transform of the step response by $j2\pi x$.

a. Experimental Considerations. The step response data were acquired using existing equipment and the geometry currently used for high-speed aero-ballistics photography. The experiment was conducted at the center and at the four extremities of the field of view. Data from the four off-axis locations will be used to evaluate lens anomalies--a factor that increases as the radial

10
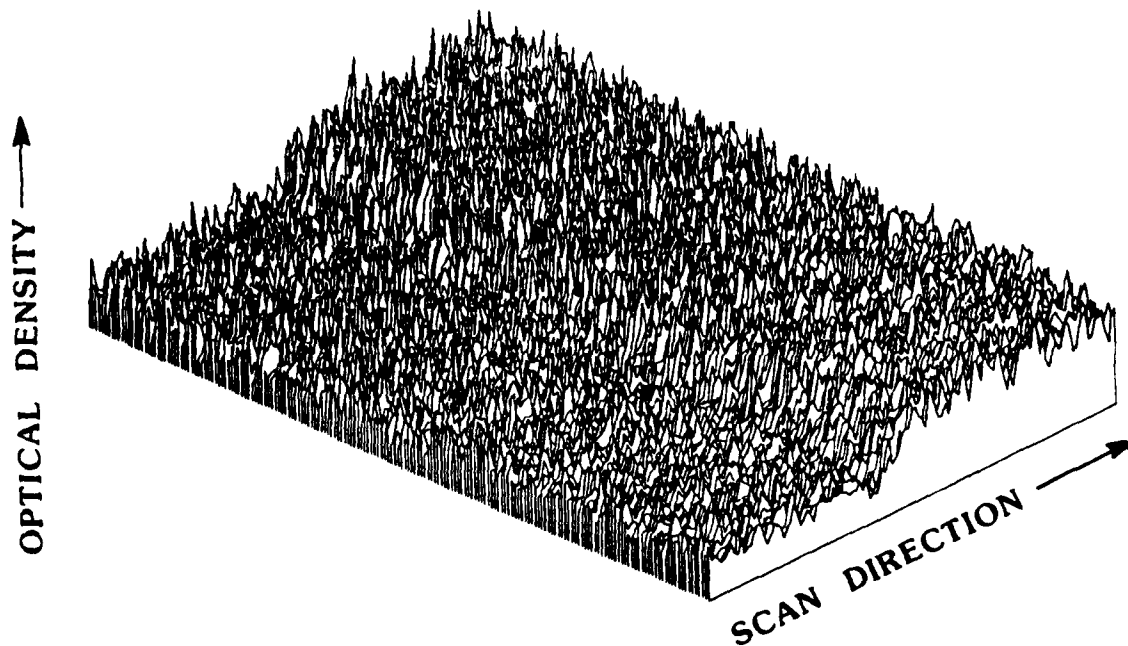
Figure 5. Digitization of Step Response as Recorded on Film (Sampling interval is 4 μm)
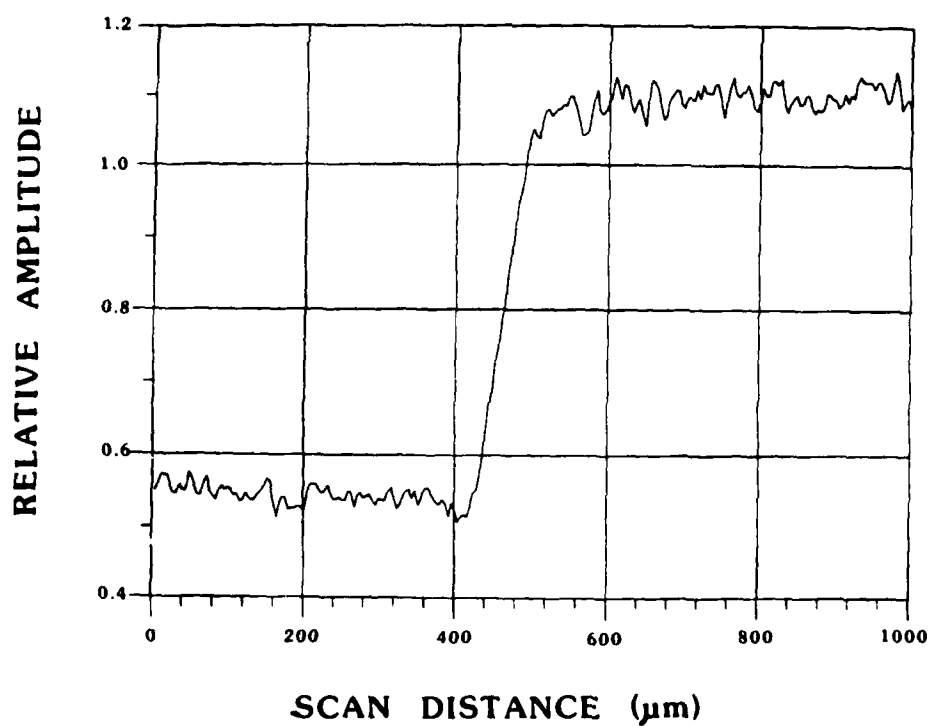
Figure 6. Average Response to Step Input

distance from the optical axis increases. Our experiment was conducted at several different photographic stations with multiple exposures at each station for statistical validity.

Physically, the step response was recorded on film using standard equipment and operating procedures. The data were prepared for computer processing by digitizing the photograph using a Perkin-Elmer scanning microdensitometer. The step response was scanned a number of times at 4-μm increments (Figure 5); then an average of all scans (Figure 6) was used for further processing.

b. Analysis. A plot of the off-axis system transfer function [or modulation transfer function (MTF)] is shown in Figure 7. This plot indicates the normalized system response versus frequency in cycles per millimeter at the object field. The goal here is to provide a reasonable estimate of the dimensions of the smallest object that can be resolved. Studies (Reference 3, page 119) have indicated that the eye normally requires an image contrast of about 3 percent to resolve light-to-dark transitions. On a normalized MTF, this contrast value is the spatial frequency at which the response has fallen to 3 percent of the passband amplitude; this frequency is called the limiting resolution.

FREQUENCY (CYCLES/mm)
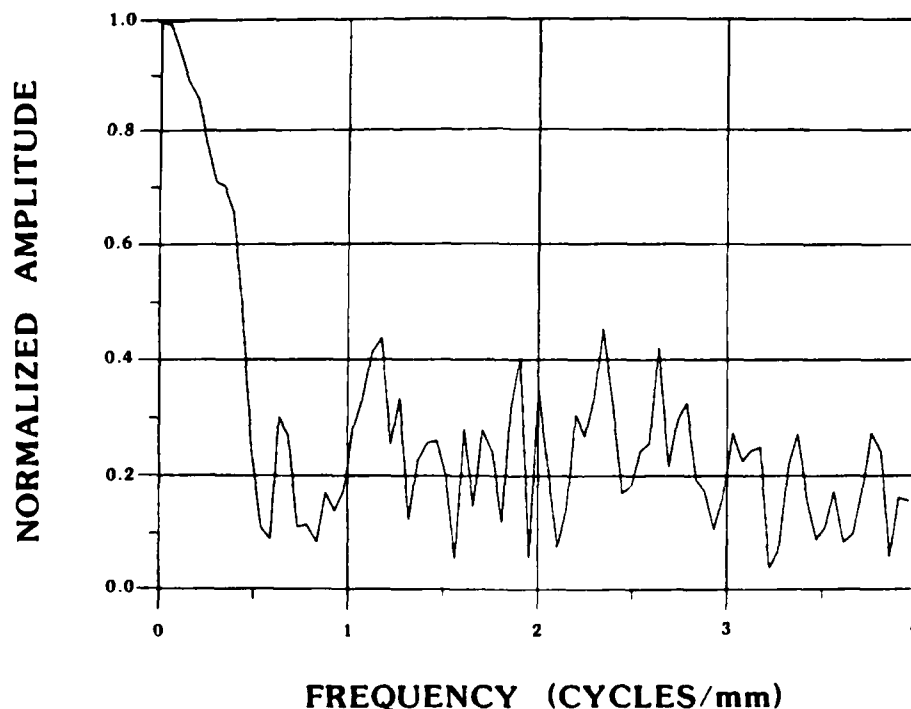
Figure 7. System Transfer Function at the Extreme Boundary of the Field of View
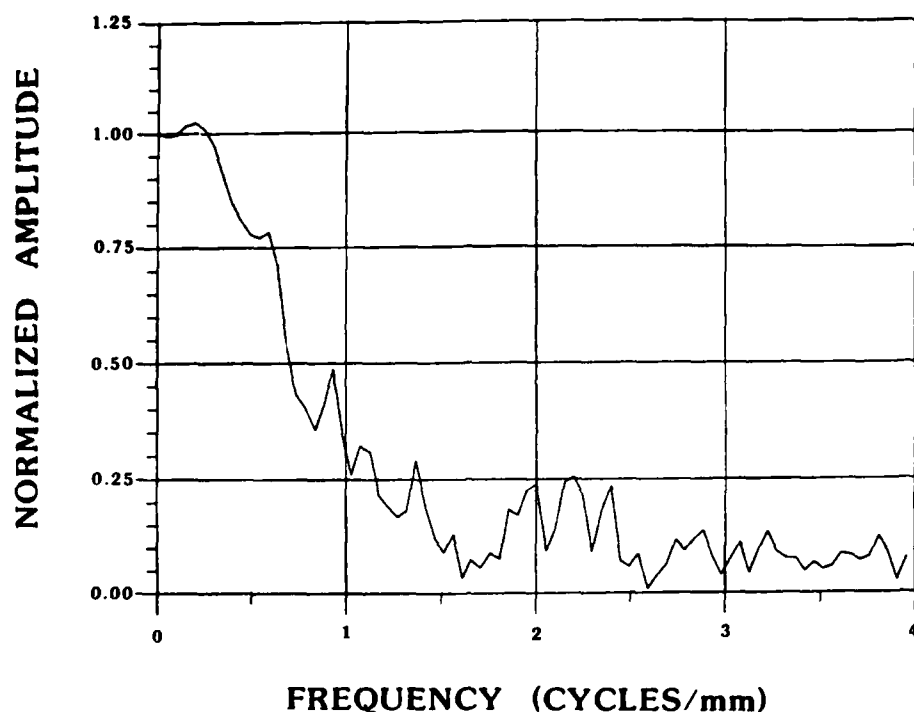
Figure 8. System Transfer Function at the Center of the Field of View (on the optical axis)

The center field frequency response is shown in Figure 8. Taking the lower frequency limit as the lowest noise-free point yields a value of 0.742 cycles per millimeter. Using this value as the zero reference boundary, we calculated the limiting resolution to be 0.72 cycles per millimeter. One industry standard for system specification is the contrast transfer function (CTF) that has square wave basis functions instead of sine waves. CTF can be calculated from the MTF by

$$CTF = C(N) = \frac{4}{\pi}\left[M(N) - \frac{M(3N)}{3} + \frac{M(5N)}{5} - \frac{M(7N)}{7} + \frac{M(9N)}{9} \ldots\right].$$

The equation yields 0.84 line pairs per millimeter for C(N) at the center of the field. In comparison, the corners will resolve about 0.5 line pairs per millimeter. This difference is due to nonlinear lens effects that increase with radial distance from the optical axis. Graphically, this difference can be seen in the differing cutoff frequencies between the off-axis transfer function of Figure 7 and the on-axis transfer function of Figure 8.

A quick way of verifying the CTF resolution derived here from experimental data is to calculate the theoretical system resolution (N_s). This is determined from all elements in the optical chain, up to and including the film,

$$\frac{1}{N_s^2} = \sum_{i}^{J} \frac{1}{N_i^2} \quad .$$

As an estimate, the major components can be used in this evaluation,

$$\frac{1}{N_s^2} = \frac{1}{N^2_{lens}} + \frac{1}{N^2_{screen}} + \frac{1}{N^2_{film}} \quad ,$$

$N_{lens} = 1.7$ lp/mm[*] (lp = line pairs at object field), and

$N_{film} = 5.2$ lp/mm .

N_{screen} The lens dimensions on the 3M Scotchlite Brand 7610 reflective sheeting determine N_{screen}. Per manufacturer's literature, these lenses are 2/1000 inch in diameter. They then constitute a resolution element equal to 2/1000 in. x 25.4 mm/in. = 5.08×10^{-2} mm, or 9.8 lp/mm.

Then,

$$N_s = \left[\frac{1}{1.7^2} + \frac{1}{5.2^2} + \frac{1}{9.8^2} \right]^{-1/2}$$

$$= 1.59 \text{ lp/mm} \quad .$$

This number (N_s) does not take into account second-order effects such as screen nonuniformities and film developing and is therefore an optimistic figure of resolution. The fact that this number is relatively close to the empirically derived 0.84 lp/mm lends additional credibility to the data.

---

[*]For a 7-in. Aero Ektar lens at an f-stop of 2.5 Optical Image Evaluation, Proceedings of NBS Semicontinental Symposium, Circular 526, p. 193.

DISTANCE (mm)
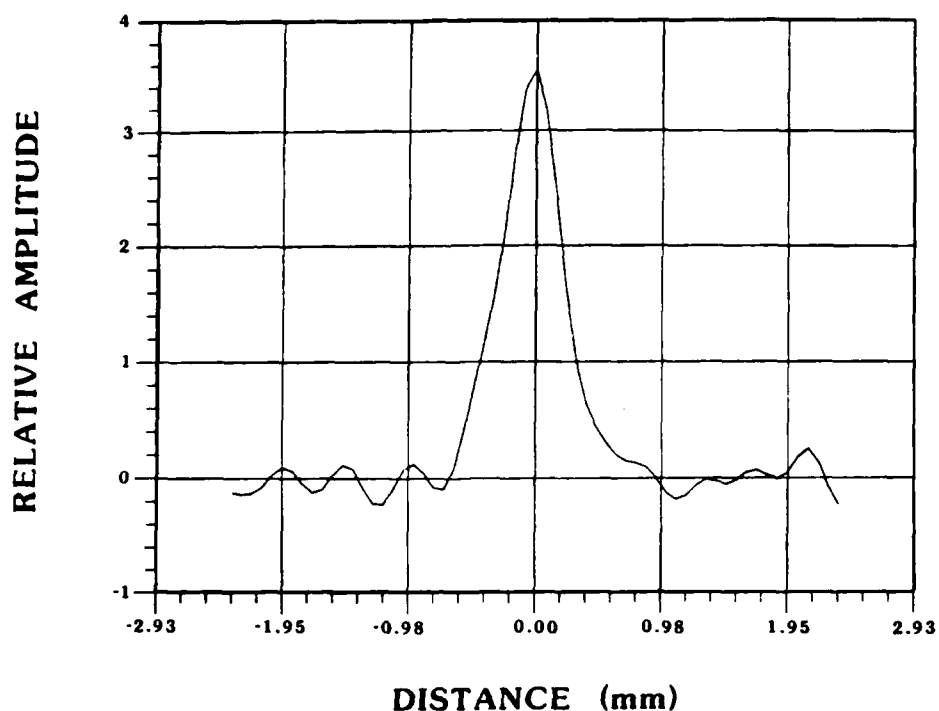
Figure 9. Impulse Response at Center Field

Another common reference figure, the minimum aperture width, can be determined from the impulse response of the system (Figure 9). The aperture width is the mimimum resolvable spot diameter and is equivalent to the width between the half-power points of the impulse response. This point is at a relative amplitude of 1.2 on the impulse response plot and corresponds to an aperture width of 0.7 mm (the width of the pulse at an amplitude of 1.2).

Although the limiting resolution and aperture width refer to absolute limits on system performance, a considerable amount of research, Reference 4, has been done on the required resolution for designated tasks. This research is interesting because the system end result is an image that must be analyzed by an operator. Table II, which summarizes the results, indicates that the system-limiting resolution should be decreased (divided) by the factor of Table II for a given task. For example, to specify the orientation of an object, the operator would require 1.4 line pairs per minimum target dimension. This dimension essentially reduces the limiting resolution to 0.84 divided by 1.4 or 0.6 lines per millimeter. The minimum target dimension for orientation specification is the inverse of this result or 1.67 mm (with respect to the object field).

15

TABLE 2.   OBSERVED LIMITING RESOLUTION

Task	Line Pairs per Target Minimum Dimension
Detection	1.0 ± 0.25 line pairs
Orientation	1.4 ± 0.35 line pairs
Recognition	4.0 ± 0.8 line pairs
Identification	6.4 ± 1.5 line pairs

(a)   (b)
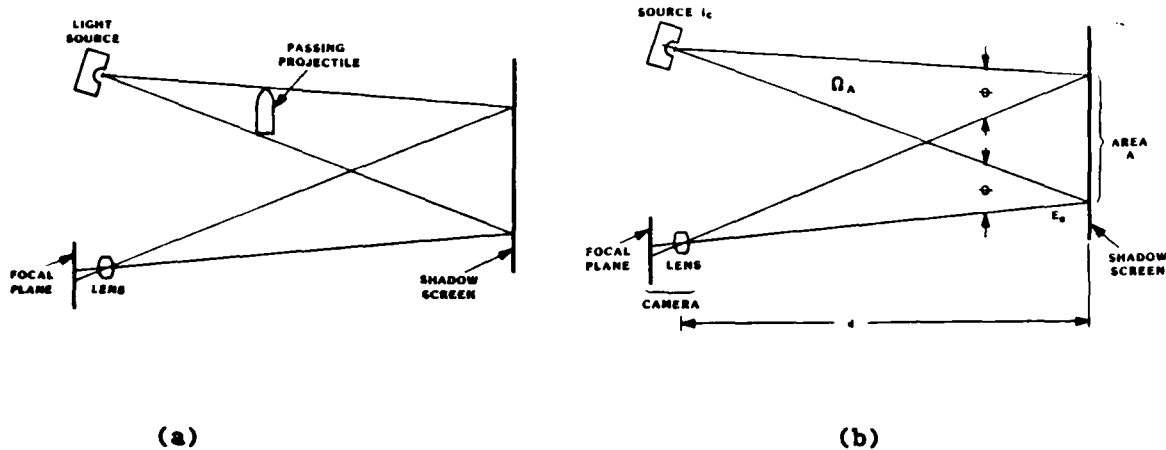
Figure 10.   Shadowgraph Geometry

4.   ILLUMINATION

Requirements of the Shadowgraph Ballistics Range, Aeroballistic Research Facility (ARF), Air Force Systems Command, Eglin Air Force Base, Florida, will be used to evaluate illumination. As Figure 10(a) shows, a pulsed light source casts the shadow of a passing projectile onto a screen at the far side of the test channel. A camera located near the light source is focused on the shadow. The light source is designed to be a point source of light so that the projectile casts a sharply delineated shadow. Also, the light source must have a very short duration to precisely time the passing projectile.

Using Royal X-Pan (Eastman) film, we obtained adequate exposures. However, neither the aeroballistics facility nor the light-source manufacturer had detailed light-source intensity specifications. To determine the usefulness of the available light for our purposes and for other imaging sensors, such as television cameras, we needed to evaluate intensity and spectral distribution; therefore, the light source was brought to Los Alamos for that evaluation.

In the following paragraphs, we establish the measurements required to evaluate the light source and describe data collection and analysis and interpretation of that data.

a. Determination of Measurement Requirements. Radiometric units will be used. In Figure 10(b), the radiant intensity I_e of the source, in watts per steradian, is related to the radiant flux ϕ_e falling on an area A of the shadow screen and the irradiance E_e (W/m^2) of that area by

$$\phi_e = I_e \Omega_A = E_e A \text{ watts} , \tag{5}$$

where Ω_A is the solid angle subtended by A in steradians. This relation assumes that E_e is uniform over A. Then

$$\Omega_A = \frac{A}{d^2} , \tag{6}$$

whence

$$E_e = \frac{I_e \Omega_A}{A} = \frac{I_e}{d^2} . \tag{7}$$

The light E_{fp} received at the camera focal plane is

$$E_{fp} = \frac{E_e R(\Theta) T}{4F^2(m + 1)^2} = \frac{I_e R(\Theta) T}{4d^2 F^2(m + 1)^2} \, W/m^2 . \tag{8}$$

In Equation (8),

   R(Θ) is the reflectance of the shadow screen at angle Θ between
          camera and light source;

   T   is the lens transmission;

17

F   is the aperture of the lens [that is, F = f/D,

       where

              f is the lens focal length and

              D is the lens diameter (really the diameter of its entrance
              pupil)]; and

m   is the magnification from object $\underline{O}$ (shadow) to image $\underline{I}$ at focal
       plane (that is, m = I/O).

   b. Parameters at Eglin. The magnification, F-stop, and transmission of
the lens at Eglin are

   m = 0.0519, F = 2.5, and T = 0.8   .

To be consistent with the values for $\underline{m}$ and $\underline{A}$ and to have a 18.4-cm
(7.5-inches) focal length, $\underline{d}$ can be shown to be 3.52 m (139.2 inches).

   At least one lens element will be of lime glass for which the transmis-
sion drops rapidly outside the 360- to 4000-nm range.
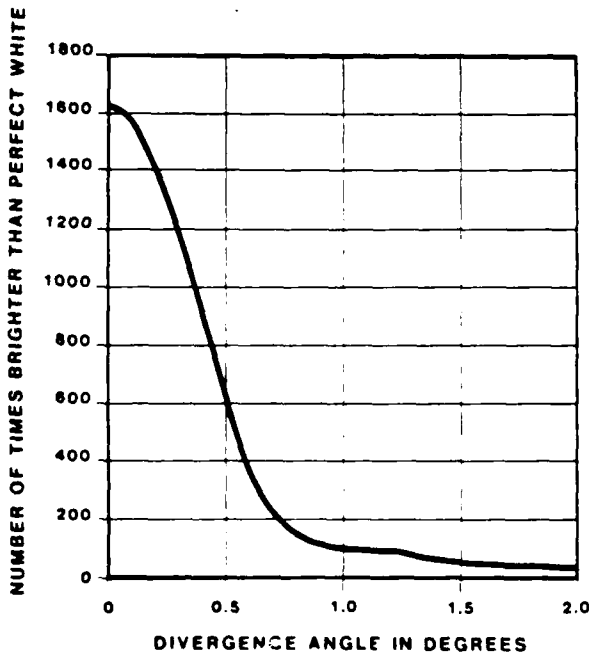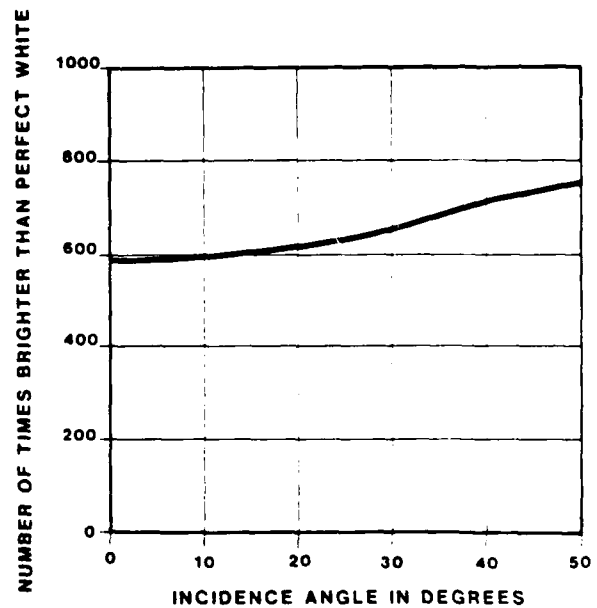
(a)   (b)

Figure 11.   Shadow Screen Reflection.   (a) Directional reflectance versus
divergence angle at 0 degree incidence of 3M No. 7610 high-intensity
reflective sheeting.   (b) Directional reflectance versus incidence angle
at 0.5 degree divergence of 3M No. 7610 high-intensity reflective
sheeting.

c. Shadow Screen Reflectance. The shadow screen at Eglin is fabricated of 3M No. 7610 high-intensity reflective sheeting. This material has a reflection gain over standard diffuse (Lambertian) white. Figure 11(a) shows the gain as a function of divergence angle Θ. The reflectance changes very little for oblique incidence out to 20 degrees, as Figure 11(b) shows.

To achieve high reflectance gain, Θ should be small; that is, the camera and light source should be as close together as possible. At Eglin, light source and camera sizes set the minimum space between the two at about 18 cm.* For this space and with 3.52 m for $\underline{d}$, Θ ranges from a minimum of 1.2 degree to a maximum of 3 degrees for which $20 < R(\Theta) < 100$ (if we presume to safely extrapolate the curve of Figure 11(a) out to 3 degrees).

d. Focal Plane/Source Intensity Relation at Eglin. Assuming $R(\Theta)$ averages 60 and the other values determined in Equation (8), we have

$$E_{fp} = 0.139I_e \text{ (at Eglin)} \quad . \tag{9}$$

e. Source Intensity Determination. A spectroradiometer having well-defined input geometry so that spectral intensity could be determined in a single set of measurements was not available. Therefore a relative spectral distribution was determined using a Tracor Northern TN-1710-25 Grating Spectroradiometer equipped with a TN 123-32 head. Total energy output in a known geometry with a photodiode of known spectral sensitivity was determined with a Photodyne 1500XP. Methods used to extract the required data are described below.

(1) Relative Spectral Distribution. The light source was perpendicular to the entrance slit of the spectroradiometer and far enough away that its output did not saturate the spectroradiometer sensor. The sensor, a linear charge-coupled device (CCD) array located at the output of the grating, stores charges proportional to the spectral distribution for read-out after the light pulse has occurred. The spectrum obtained is therefore the average spectral distribution during the pulse.

---

*Camera and light source cannot be made coincident, for then the camera would see only the projectile and not the projectile's shadow.

The relative spectrum $S(\lambda)$ is shown in Figure 12. The ordinate is $GI_e(\lambda)R(\lambda)$, where $\underline{G}$ is an unknown calibration factor, $I_e(\lambda)$ is in watts/steradian-nanometers, and $R(\lambda)$ is the responsivity of the CCD in amperes/watt. The latter information is available from the manufacturer in terms of CCD quantum efficiency. The responsivity and quantum efficiency $\eta(\lambda)$ have the following relation (Reference 3, page 149).

$$R(\lambda) = \frac{e\lambda\eta(\lambda)}{hc} \quad . \tag{10}$$

The output now becomes

$$S(\lambda) = G'\lambda\eta(\lambda)I_e(\lambda) \quad , \tag{11}$$

where G' includes the e/hc factor. Values $\eta(\lambda)$ for the CCD are plotted versus wavelength in Figure 13.
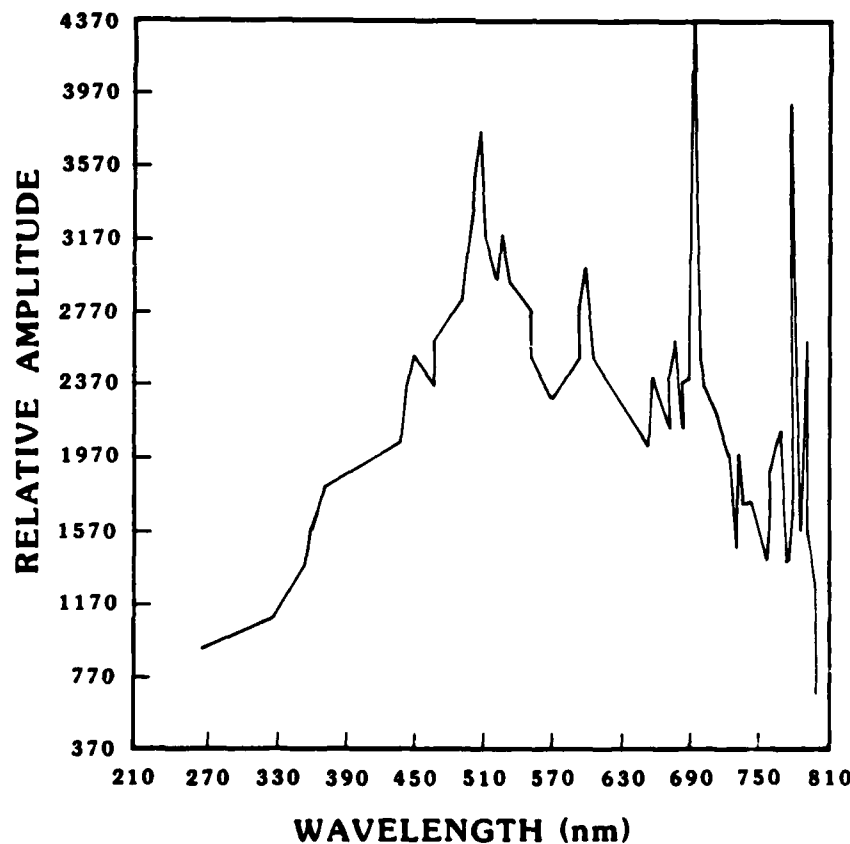
Figure 12. Relative Spectra

20
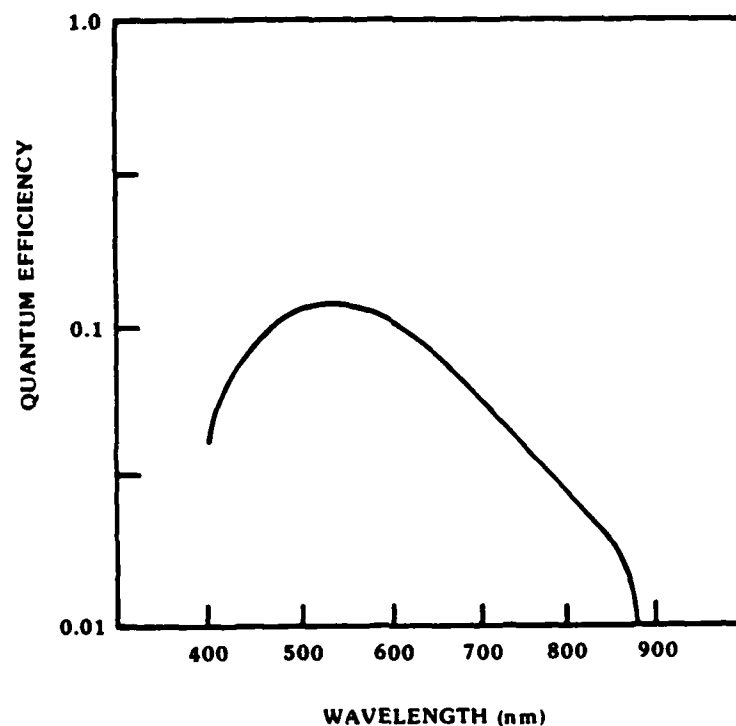
Figure 13. Quantum Efficiency of the Spectroradiometer

The Figure 12 abscissa was originally unscaled. The three dominant spectral lines were identified by comparison with known sources: 770 nm from oxygen, 656 nm from hydrogen, and 501 nm from nitrogen. From these value· ·e scale was determined.

Normalizing the responsivity-corrected relative spectral values $S(\lambda)$ to those at a selected wavelength N, we get

$$\frac{S(\lambda)}{S(N)} = \frac{G'\lambda\eta(\lambda)I_e(\lambda)}{S(N)} \tag{12}$$

from which

$$I_e(\lambda) = \frac{1}{\lambda\eta(\lambda)} \times \frac{S(\lambda)}{S(N)} \times \frac{S(N)}{G'} \quad . \tag{13}$$

The spectrum, corrected for responsivity wavelength dependence, was normalized for N = 710 nm, where the amplitude equals 71.7. The result is plotted in Figure 14.
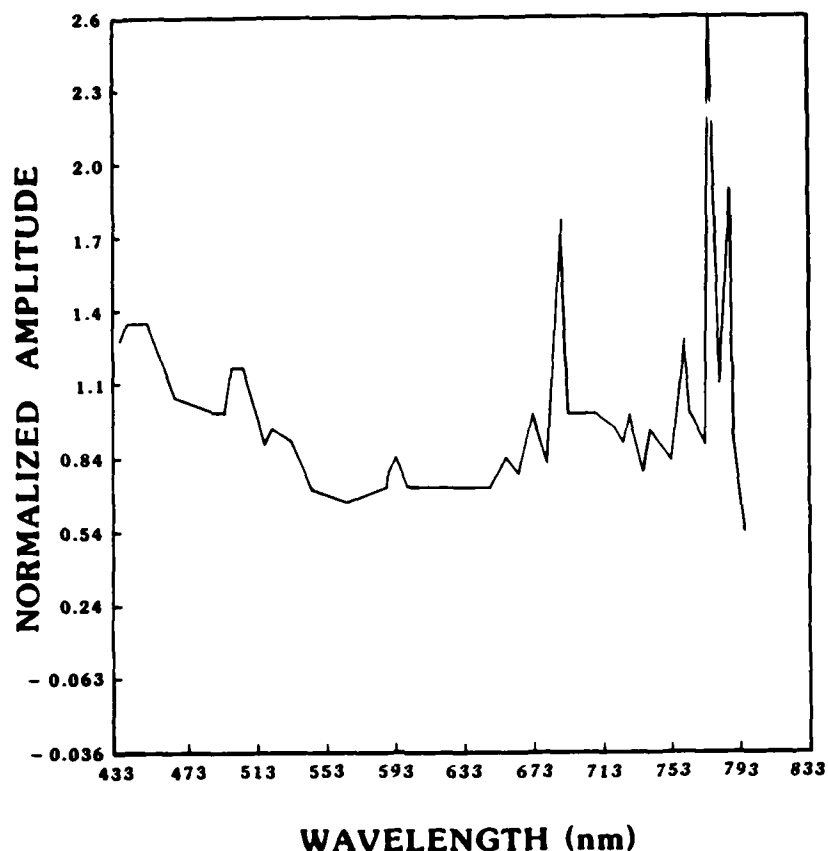
Figure 14. Corrected Normalized Spectrum

In Equation (13), all factors are known except G', which shall be determined from the total radiant energy measurement described in the following section.

(2) Total Radiant Energy. A Photodyne 1500 XP radiometer measured total radiant energy. The light-source axis was aligned perpendicular to and centered on the photodiode sensitive surface. The sensitive surface (diameter $\underline{a}$ = 2 mm) was located at a distance $\underline{s}$ ($\underline{s}$ = 65.4 cm) from the light source. The radiometer output is wavelength dependent and is in P(λ) V/W $\underline{if}$ only the sensitive area (or less) is irradiated. When more than the sensitive area is irradiated, as in this measurement, the radiometer output units should be changed to a new value P'(λ) in volts/watt $\pi a^2/4$, where $\underline{a}$ is now in meters.

22
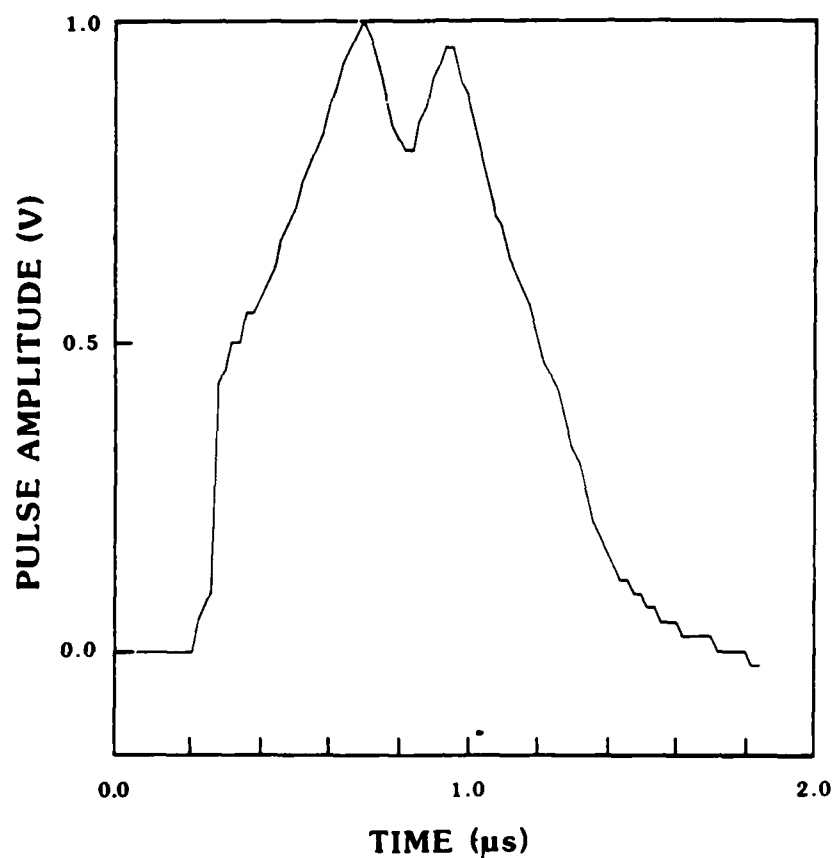
Figure 15. Radiometer Output

The output, a time-dependent voltage corresponding to the light pulse, is

$$v(t) = \int_{\lambda_1}^{\lambda_2} P'(\lambda)i_e(\lambda,t)\Omega_a d\lambda \quad , \qquad (14)$$

where Ω_a is the solid angle subtended by $\underline{a}$ and $i_e(\lambda,t)$ is the
time-dependent spectrum of light received. Figure 15 shows voltage pulse.

The spectroradiometer measure $I_e(\lambda)$ is the time integral of
$i_e(\lambda,t)$. Therefore, for comparison the radiometer output must be inte-
grated. (This comparison eliminates questions ___ _ut the time dependence of
the spectral distribution.)

23

When we integrate, Equation (14) becomes

$$\int_0^{\Delta t} v(t)dt = \int_0^{\Delta t}\int_{\lambda_1}^{\lambda_2} P'(\lambda)i_e(\lambda,t)\Omega_a \, d\lambda dt = \int_{\lambda_1}^{\lambda_2} P'(\lambda)I_e(\lambda)\Omega_a\Delta t \, d\lambda \quad ,$$

where $I_e(\lambda)$ is the average spectral distribution of Equation (13) and Δt is the pulse length. We insert Equation (13) in Equation (15):

$$\int_0 v(t)dt = \int_{\lambda_1}^{\lambda_2} P'(\lambda) \, \Omega_a \left[\frac{1}{\lambda\eta(\lambda)} \frac{S(\lambda)}{S(N)}\right] \left[\frac{S(N)\Delta t}{G'}\right]d\lambda \quad , \tag{16}$$

where the bracketed value is the normalized spectrum. But $P'(\lambda) = P(\lambda)/\pi a^2/4$ and $\Omega_a = \pi a^2/4s^2$; hence, Equation (16) becomes

$$\int_0 v(t)dt = \frac{S(N)\Delta t}{s^2 G'} \int_{\lambda_1}^{\lambda_2} P(\lambda)\left[\frac{1}{\lambda\eta(\lambda)} \frac{S(\lambda)}{S(N)}\right]d\lambda \quad . \tag{17}$$

Figure 16. Normalized Radiometer Sensitivity

A normalized curve $P(\lambda)$ referred to the sensitivity at 810 nm, where $P(\lambda) =$ 1 mV/μW (Figure 16). Then $P(\lambda) = P(810) \times P(\lambda)/P(810)$, and Equation (17) becomes
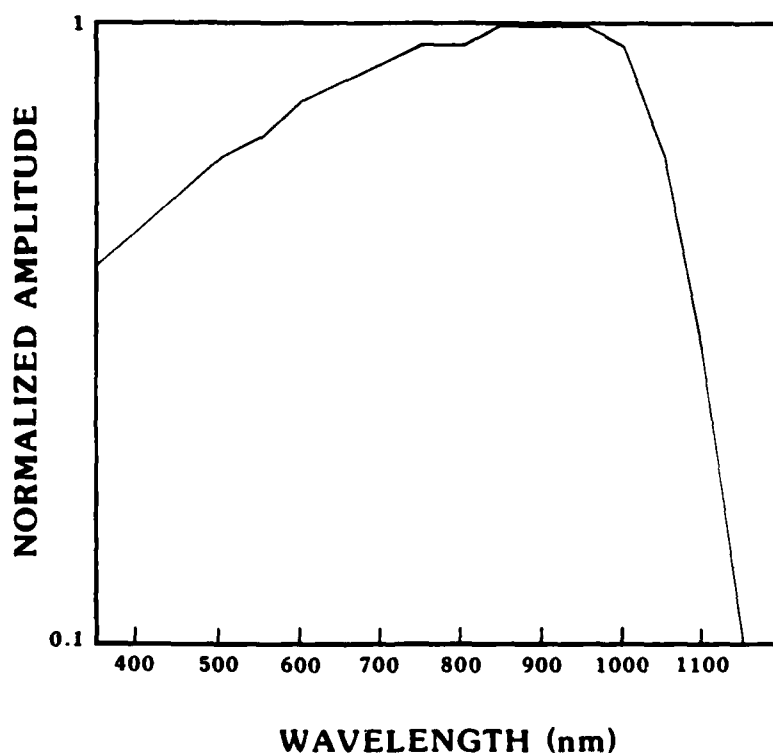
$$\int_0^{} v(t)dt = \frac{S(N)P(810)\Delta t}{s^2 G'} \int_{\lambda_1}^{\lambda_2} \left[\frac{P(\lambda)}{P(810)}\right]\left[\frac{1}{\lambda \eta(\lambda)}\frac{S(\lambda)}{S(N)}\right]d\lambda \quad . \tag{18}$$

In Equation (18), all values are known except G'. The two brackets are values for the normalized radiometer response and the normalized spectrum. When we solve for G',

$$G' = \frac{S(N)P(810)\Delta t}{s^2} \quad \frac{\displaystyle\int_{\lambda_1}^{\lambda_2} \frac{P(\lambda)}{P(810)} \left[\frac{1}{\lambda\eta(\lambda)}\frac{S(\lambda)}{S(N)}\right] d\lambda}{\displaystyle\int_0^{\Delta t} v(t)dt} \quad . \tag{19}$$

The value of the wavelength integral for $\lambda_1 = 432$ nm to $\lambda_2 = 792$ nm is 240. The value of the time integral is 0.717. For the radiometer sensitivity scale, we used $P(810) = 1$ mV/μW or 10^3 V/W. When we substitute $\underline{s}$ and the other values now determined, $G' = 16.8$.

Referring to Equation (13), we now can describe the spectrum $I_e(\lambda)$ as

$$I_e(\lambda) = \frac{S(N)}{G'} \times \text{the responsivity-corrected and normalized spectrum}$$

$$= 4.27 \times \text{the normalized spectrum of Figure 10.}$$

f. Illumination Conclusion. The spectral radiant intensity of the light source is now determined. For use with any imaging sensor, all that is needed is the responsivity of that sensor. The term $I_e(\lambda)$ is a general-purpose statement of light-source spectral output and will be used further in system design and specifications. Information derived from the resolution analysis can be coupled with this result to encompass system parameters and maximize S/N ratio for optimum system performance.

5. EI SYSTEM CONSIDERATIONS

A number of possibilities exist for replacing film cameras with EI hard-
ware; each possibility will match imaging requirements established in previous
sections. However, processing strategies and associated hardware will vary
dramatically for each method. In all cases, electronics must be associated
with the EI unit to control its operation and store the image data. The
storage function is necessary to permanently archive the image. EI devices
are only capable of retaining image data for a short time before data degrada-
tions occur; therefore, associated electronics must be able to store the image
data at video or near-video rates. Figure 17 shows a configuration for an EI
subsystem that would replace the present film camera. The external communica-
tion link provides a data path from each EI subsystem to a central data col-
lection computer (host computer) as shown in Figure 17. The host computer is
responsible for collecting, maintaining, and analyzing the images from each EI
subsystem. For each image, the analysis would consist of finding the critical
points and the projectile and establishing the coordinates of those points.
The coordinate would be in respect to the reference beads at the top and
bottom of an image. In addition, the host computer would control each EI
subsystem for pre- and post-shot operations.

a. EI Subsystem. The purpose of the EI subsystem is to record an
image. The operator normally has access to the images after the host computer
has read the images from each subsystem (or station). The major components
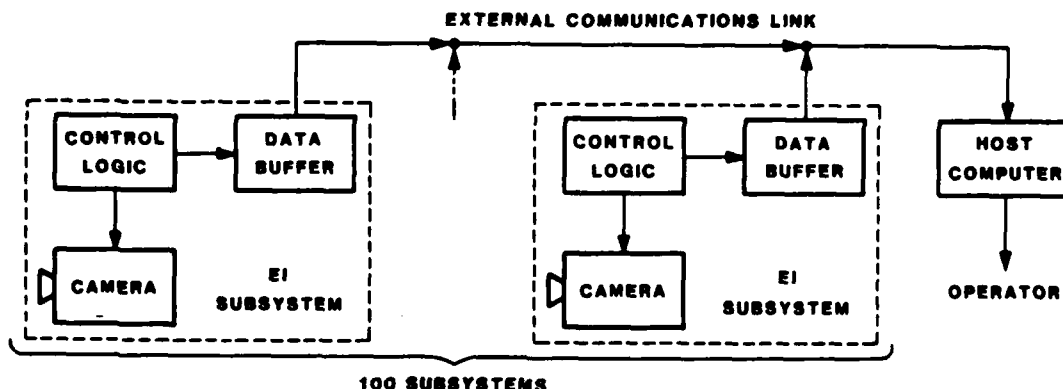

Figure 17.   The EI Subsystem Acquires and Temporarily Stores the Image
             Data. The host computer collects all images over a high-
             speed data link for presentation to the operator.

26

(Figure 17) are the EI device (or camera), control logic, and data buffer. During a typical test shot control sequence, control logic would accept commands from the host to prepare the substation (that is, the camera scrub cycle, etc.). The existing infrared detector system would activate the camera. Immediately after the projectile is imaged, the control logic transfers the image from the camera to the data buffer. The data remain there until the host accesses the subsystem.

Several options exist at the subsystem level and several types of cameras can be used. (They are discussed in paragraph F) In each case, the rate at which data can be read is variable. To maintain resolution, data must be accessed as quickly as possible. Currently, available control and data buffer hardware will operate at approximately 13 million bytes per second. This means that an image will be read from the camera within approximately one-half second, which is acceptable to slow-scan camera technology.

The control logic and data buffer can be implemented with standard, commercially available products; custom-built hardware; or some combination of both. Using commercial products is expensive, but such use minimizes design risks, and the products are usually backed by warranty and a maintenance organization. Custom hardware can be much cheaper when purchased in quantity and can perform better, but usually it is not backed by a maintenance organization (that is, users must do their own maintenance).

For the aeroballistics range, custom hardware would be much cheaper than a commercial product because the hardware would be designed specifically for the EI subsystem and therefore would require less hardware than a general-purpose commercial unit; and, Los Alamos is not profit structured and therefore the hardware could be bought at cost.

Primarily, hardware optimization would be developed around data compression techniques. These methods will work expecially well in the EI subsystem because an image is composed of a projectile and two Kevlar lines; all remaining data could be suppressed, thereby drastically reducing the size of the data buffer. The compression techniques used would be the so-called error free methods so that the image resolution would be unchanged.

b. Host Processor. The host processor will act as a data collection point for all of the EI subsystems. The processor should be a high-speed, general-purpose micro- or minicomputer with a large mass-storage device for

27

storing images and a tape drive for permanent data archival. A high-resolution graphics terminal would be needed to display the images, and an image-quality hardcopy unit may be desirable to produce prints of the images.

The host processor could work in a number of modes. The simplest mode would interface with existing equipment to get preshot timing information to ready the EI subsystems. In this case, the host could interface with the ASIA controller so that control currently associated with opening the camera shutters c,uld be used to initiate commands from the host to the subsystems to prepare for the shot. A more complicated route could consist of an integrated approach to the aeroballistics facility. This mode would take advantage of some of the power of a general-purpose computer to collect not only image data but also the data now collected by HERMN (including timing data). In addition, control functions now done by ASIA could be done by the host. Therefore, with this approach, the same computer that performs the image processing could replace the current HP computer and the ASIA. This integrated approach would ease maintenance requirements and provide a simplified operator interface, but it would require more design engineering than the simpler approach.

The operator will command all of the EI system functions from the host console. After a shot, the host will access the EI subsystems in a sequential fashion. Image data will be transferred over a very high speed data link and be stored on disk. The time required to transfer 100 images over the data link depends on the speed of the link and whether data compression is used. We recommend that data compression be used; otherwise, approximately 10^9 bytes of data must be transferred and stored on the host. After transfer is complete, the operator may start analyzing the images. We envision that the operator, using a light pen, will be able to roughly indicate critical points on the image, as shown in Figure 18. The host will use these approximate indications to find, by means of advanced pattern classification techniques, the exact coordinates of the critical points. In other words, the operator must indicate the approximate locations of the critical points within a certain error radius, as shown in Figure 19. The host could then display the numerical value of the exact point locations along with cross-hair indicatirns of where the final points are on the projectile. This feature would reduce the time required to process each image, but more importantly, it will give

the resulting set of data from all stations a consistency that cannot be achieved through manual operations. As a result of this consistency, the effective accuracy of the system is increased.

When the operator has processed all images, the data can be put on tape in a format compatible with the existing method and then transported to a larger computer for further analysis as is presently done. The image data could also be put on tape and/or printed on an image-quality hardcopy unit. Quick-look data could also be made available, such as a movie mode. In this mode the sequence of 100 images would be aligned and displayed in rapid sequence, thus giving the researcher a quick idea of the projectile flight path.

c. Maintenance. Commercial products such as the host computer can be maintained either by company service representatives or by ARF personnel. Routine maintenance like tape head cleaning and camera adjustments would be reasonable tasks for ARF personnel. In fact, it seems reasonable that the current level of personnel at the ARF could deal with a majority of the problems that may arise. Modern computer systems typically have on-board diagnostics that take some of the guesswork out of troubleshooting. In addition, a certain amount of maintainability can be built into the EI system. For example, Figure 20 demonstrates how local EI subsystem adjustments can be made. A technician may do maintenance by connecting a portable monitor to a particular EI subsystem. The monitor would display exactly what the camera sees so that adjustments in the focus or camera alignment could be made.

6. TELEVISION REQUIREMENTS

In television systems the optical system forms the image on a photoactive surface (photocathode), where electrical charge released is read out by a scanning electronic beam in all tube-type image sensors (vidicons, etc.) or by a charge transfer process in photosensitive array devices [CCDs and charge-injected devices (CIDs)]. Initially, our discussion will be devoted to the tube-type image sensor; the terminology developed will be directly applicable to the imaging array devices.

The system of scanning lines is known as the raster. Except for special uses that are not applicable here, the scanning lines are straight and parallel. Interlaced scanning, employed in the television industry to reduce flicker, will not be employed here. Adjacent lines will be adjacent in time.

The resolution perpendicular to the scanning lines is determined by their spacing, the reading beam profile, and the point-spread function of the optics. The resolution along a scanning line determines the required video bandwidth.

a. **Raster Design.** The raster will read a rectangular area on the image tube that corresponds to the field of view at the object plane. The scanning lines can be along either dimension of the raster. Both schemes will be examined so that the one requiring the lower video bandwidth (and therefore less video noise) may be selected. The actual raster dimensions at the image tube will be determined by the photocathode dimensions, which in turn will determine the lens to be employed. The image tube cannot be selected until the aspect ratio and vertical and horizontal resolution requirements are determined. Therefore, these measurements will be determined in the object field.

(1) **Object Field Dimension.** The object field at the reflecting screen is somewhat smaller than the screen and is determined by the exposed part of the film in the camera. The relation between the two sets of dimensions will be determined by the camera magnification m. The distance between the fiducial beads at the screen, 91.44 cm, was used as a reference. On one test film employed to determine the MTF and the line-spread function, the images of these
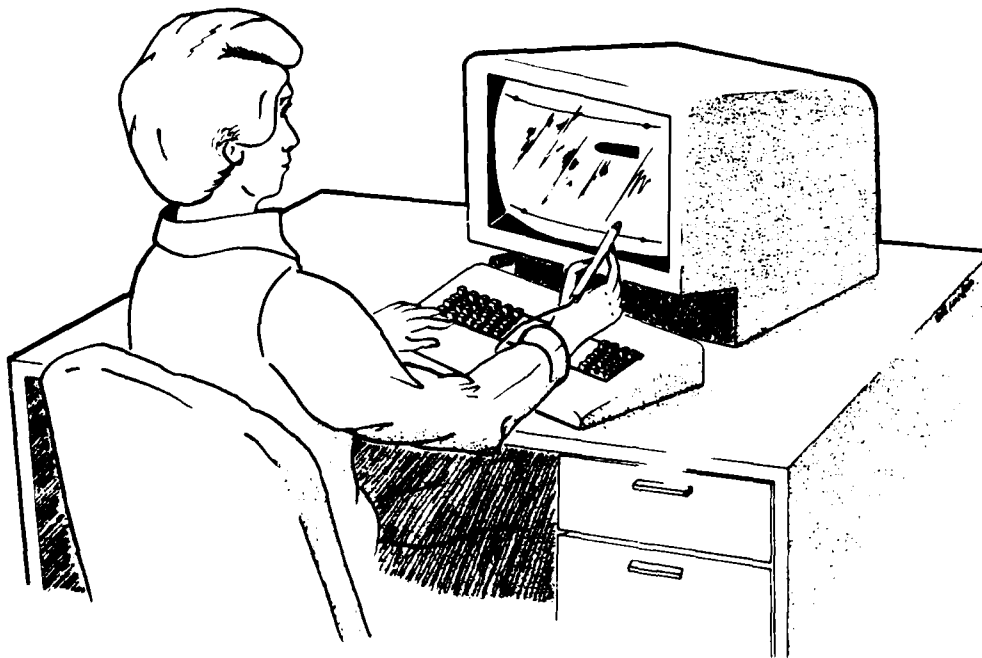
Figure 18. Analysis of Imaged Data at the Host Computer Console.
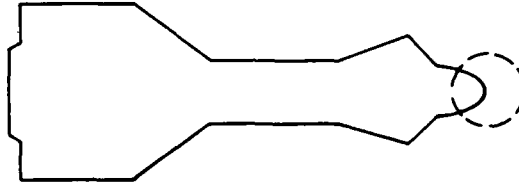
Figure 19.   Tolerance Radius in Critical Point Selection

beads were spaced 4.746 cm apart.   The image-to-object (I/O) magnification, that is, m = I/O, was 0.0519.   (This magnification varied somewhat from camera to camera.)

The horizontal and vertical dimensions of the exposed part of the film were 5.842 cm and 12.09 cm, respectively.   Hence, in the object field,

H = 5.842/m = 112.6 cm or 1126 mm, and

V = 12.09/m = 232.9 cm or 2329 mm.
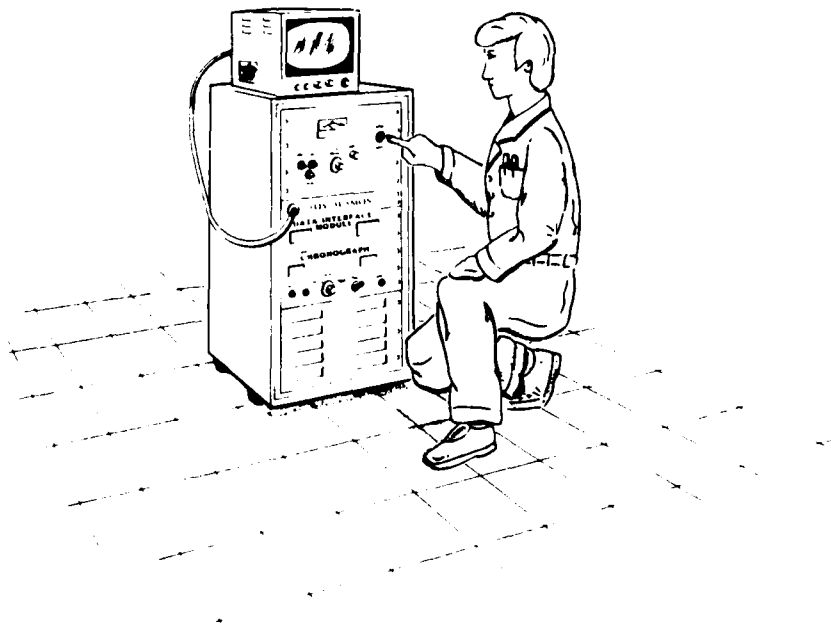
Figure 20.   Local Maintenance on an EI Subsystem.

31
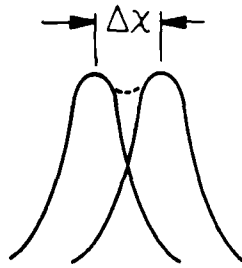
Figure 21. System Aperture Width.

The aspect ratio V/H will be 2.069:1 if the scanning line is along the horizontal dimension or 0.483:1 if it is along the vertical dimension.

(2) Object Field Resolution. The point-spread function is the image formed by the system from a point source of light. As two-point sources of light are brought closer together, the limit of the system's ability to resolve the two is reached when their spacing Δx is equal to the half-power width of the point-spread function. As shown in Figure 21, the resulting signal (the dotted line) is one television line. In paragraph II.3.b., Δx was determined to be 0.7 mm in the object field.

The number of cycles required in each direction will then be

$$N_H = \frac{1126}{0.7} = 1608 \text{ television lines and}$$

$$N_V = \frac{2329}{0.7} = 3329 \text{ television lines.}$$

(3) Bandwidth Requirement. Each scan line will require a time t_s for completion. As noted above, the bandwidth is determined by the resolution along the scan line; that is, the bandwidths for horizontal and vertical scanning are

$$BW_H = N_H/t_s \text{ and}$$

$$BW_V = N_V/t_s \quad .$$

32

The scan times may not be the same, however. They will be determined by the total time allowed to read the raster and by the time required for interline pulses. Because only a single frame (the raster) is to be read, the normal interframe synchronizing pulses will not be required.

Standard television interline synchronizing pulses require a time of 11.11 µs. If we assume a synchronizing time of 11 µs, the time per line t_l will be

$$t_l = t_s + 11 \times 10^{-6} \quad .$$

For a total of N_R lines in the raster, the total time per raster t_R will be $N_R t_l$. The resolution perpendicular to the scan lines will be less than the number of scan lines by a factor known as the Kell factor, Reference 5. This factor, determined by the raster line spacing, the reading beam profile, and the optical point-spread function, was found experimentally to range from 0.53 to 0.85. These factors included the lines required for interframe processing in standard television. To use the modern stable raster system, which does not require interframe lines, we assume a conservative value of 0.85. For a required resolution of N_p (perpendicular to the scanning lines),

$$N_R = N_p/0.85 \quad .$$

Then the total master read-out time t_R will be

$$t_R = N_p t_l/0.85 \quad .$$

If we assume a raster read-out time of 0.3 s, the time per line will be

$$t_l = 0.255/N_p \ s \quad .$$

From the above relations the following table of values can be developed for horizontal and vertical scanning.

33

Scanning	N_R	t_s (μs)	Bandwidth
Horizontal	3917	54.1	29.7 MHz
Vertical	1892	123.8	26.9 MHz

Although the bandwidths differ little, the smaller bandwidth of the vertical scanning system will reduce the noise power by about 10 percent.

b. Selection of Image Sensor. For perfect geometry the ideal sensor would be a photosensitive array device such as a CCD or a CID. At the present time, none of the commercially available products meets the resolution requirements. However, as part of project Galileo and the space telescope, the National Aeronautics and Space Administration (NASA) is funding work on high-resolution array-type devices. A summary of known work on imaging arrays is presented in paragraph 6.e., along with some ideas for expanding the effective resolution of present devices.

Among the tube-type image sensors, only the return beam vidicon exceeds the BI resolution requirements, Reference 6. This tube is not available commercially. The Westinghouse WX-5156, designed for document reading, is capable of reading 3200 lines/scan; its MTF is 5 percent. If we extrapolate to 3 percent, as Johnson advises, Reference 7, the resolution would be 3746 lines/scan. The imaging optic, light requirement, dynamic range, and expected noise for the WX-5156 are described below.

c. Raster Dimensions. The useful diameter of the WX-5156 image tube is 35.6 mm (1.4 inch). A raster having an aspect ratio of 2.069:1 must be fitted within this circle. The raster horizontal and vertical dimensions are h and v:

$$h^2 + v^2 = 35.6^2 \text{ and}$$

$$v/h = 2.069$$

from which

$$h = \sqrt{35.6^2/(2.069^2 + 1)} = 15.47 \text{ mm and}$$

$$v = 32 \text{ mm} \quad .$$

34

In the process, extra vertical resolution is obtained. The scan line, which had a 3746 line resolution, was for a 3:4 aspect ratio, where the scan dimension was 28.44 mm. Therefore, the available resolution along the scan line will now be 32/28.44 x 3746 or 4215 lines.

Two questions must now be answered: Has the extra resolution along a scan line been obtained at the expense of resolution perpendicular to the scan line? Does the bandwidth have to be increased to take advantage of the available resolution along a scan line?

The scanning beam profile determines the maximum useful scan-line density and the resolution along a scan line when resolution is not bandwidth limited. The half-width Δb of the scanning beam profile is

$$\Delta b = \frac{\text{scan line length}}{\text{lines/scan}} = \frac{32}{4215} = 7.59 \times 10^{-3} \text{ mm} \quad .$$

The maximum useful scan line density is

$$N_{R_{max}} = \frac{15.47}{7.59 \times 10^{-3}} = 2038 \quad .$$

This value exceeds the required value for N_R (for vertical scanning) by 8 percent.

If the full resolution capability is to be attained, the bandwidth will have to be increased; that is,

$$BW_r = 4215/123.8 \times 10^{-6} = 34.0 \text{ MHz} \quad .$$

However, note that the increased resolution will be only along the scan line (vertical dimension). The resolution perpendicular to the scan lines (the horizontal dimension) will be limited to the value determined in Sec. F.1.b.

d. Imaging Optic. The required focal length can be determined from the magnification required and the lens-to-object field dimension. From the thin lens equation, we can show that

$$f = \frac{om}{1 + m} \quad .$$

35

where f is lens focal length, o = lens-to-object distance, and m = the I/O ratio. From paragraph 4.b., o = 3520 mm. The I/O ratio is 32/2329 or 0.0137. Then,

$$f = \frac{3520 \times 0.0137}{1.0137} = 47.7 \text{ mm} \quad ,$$

a value within 95 percent of the standard 50-mm focal length lens employed in 35-mm cameras. For f = 50 mm, m = 0.0144. A small compensating adjustment in the vidicon deflection optics should be possible without degradation of geometry or resolution.

At the focal plane, a resolution of 4215/32 or 132 television lines is required for full bandwidth or 3329/32 = 104 lines for minimum bandwidth. The latter is easily obtained with modern-design, off-the-shelf lenses. However, the lens resolution must exceed the complete system resolution by a sufficient margin so that lens resolution does not degrade system resolution appreciably. Component resolution N_j controls the system resolution N_s, as the following relation shows:

$$\frac{1}{N_s^2} = \sum_j^J \frac{1}{N_j^2} \quad .$$

Three known components are the lens N_ℓ, the screen N_{sc}, and the vidicon N_{vi}. In the object field,

N_{sc} = 9.8 cycles/mm, a value determined by the size of the screen lens;

$N_{vi} = mN_v$ = 0.95 cycles/mm, the maximum resolution available from the vidicon; and

N_s = (104/2)m = 0.75 cycles/mm, the minimum allowable system resolution.

Solving for N_ℓ gives the minimum admissible lens resolution:

$$mN_\ell \geq \left[\frac{1}{N_s^2} - \left(\frac{1}{m^2 N_V^2} + \frac{1}{N_{sc}^2}\right)\right]^{-\frac{1}{2}}$$

and

$$N_\ell = \frac{0.588}{0.0144}$$

$\qquad$ = 40.8 cycles/mm (with respect to the focal plane).

This value will require a high-quality lens, which can be purchased from a number of commercial sources.

Light Requirement

The minimum light will be that amount producing a signal at the limiting resolution spatial frequency, which is recognizable in the prevailing video noise. Therefore, video noise must be determined first. The final determination must compare signal and noise electron inputs with the video amplifier system--a problem in recognition statistics (Reference 3, Chapter 8).

Video Noise

With vidicon image tubes, noise in the first stage of the video system will dominate. A good video front end will have noise current input equivalent to about 7×10^{-9} A for a 30-MHz bandwidth. For white noise this input is $7 \times 10^{-9}/\sqrt{30 \text{ MHz}}$ or 1.3×10^{-12} A/Hz. For maximum resolution, the bandwidth required is 34.0 MHz. The equivalent video noise input would be

$$i_n = 1.3 \times 10^{-12}/\left(\sqrt{Hz} \times \sqrt{34.0 \times 10^6}\right)$$
$$\qquad = 7.6 \text{ nA} \quad .$$

This video noise input constitutes a noise electron arrival rate $\dot{n}_n$ of

$$\dot{n}_n = \frac{i_n}{e} = \frac{7.6 \times 10^{-9} \text{ C/s}}{1.6 \times 10^{-19} \text{ C/electron}}$$

$$\qquad = 4.74 \times 10^{10} \text{ electrons/s} \quad .$$

Picture Element Time

The time Δt, which is required to read out each picture element at maximum resolution, will be

$$\Delta t = \frac{t_s}{N_v} = \frac{123.8 \times 10^{-6}}{4215} = 29 \times 10^{-9} \text{ s} \quad .$$

During this time the noise electrons collected will be

$$n_n = \dot{n}_n \Delta t = 4.74 \times 10^{10} \times 29 \times 10^{-9} = 1392 \text{ and}$$

$$\delta n_n = \sqrt{n_n} = 37 \quad .$$

The variation in the noise electrons will be less than 3 percent; therefore, average values will be employed. Recognition statistical treatment is not required.

S/N Ratio at 3% MTF and Required Light Level

For standard broadcast television, the S/N ratio at the limiting resolution can be less than one because the eye integrates the displayed scene for about 0.2 s. This is time to correlate out the noise over 6 frames (or 12 fields). In this application a single frame will be read. Visual experience while looking at an A scope oscilloscope display of a single line of video shows that a signal having S/N = 1 cannot be seen, whereas for S/N = 3 the signal can be seen. At S/N = 2 the signal can be seen occasionally. Therefore, let S/N_{min} = 3 [that is, $n_s \times$ MTF (0.03) = $3n_n$], where n_s are the signal electrons that would be collected during a picture element time Δt _if_ the MTF was 1. Then $n_s = 3n_n/0.03 = 100n_n$, providing a dynamic range of at least 100:1 of which the system requires $n_s = 1.39 \times 10^5$ electrons.

Selection of Photoconductor

Four different photoconductors are available with the WX-5156 (Table 3). They differ primarily in spectral response and image degradation with time after exposure. All show a small rise in output until about 2 s after exposure. (This increase is probably due to the so-called soaking phenomena caused by release of charges from deep-lying sites within the photoconductor.) How much time elapses after each exposure will depend on the

38

associated computer system architecture. Therefore, tentatively, the photo-
conductor with minimum image degradation will be selected. This is photo-
conductor B that degrades in limiting resolution by 32 percent at 100 s after
exposure (Figure 22). Unfortunately, this is a less sensitive photoconductor
(Figure 23). However, the spectral response of photoconductor B (Figure 24)
is well matched considering the light source and the decay characteristics.
It peaks at 4250 Å, and the spark-gap light peaks in the blue spectral
region (Figure 14).

Signal Electrons n_s

The signal electrons will be collected during the spark-gap flash.
Except for a small increase as a result of soaking and a small loss between
exposure time and collection time, the number of electrons will be propor-
tional to the total radiance received from the light flash and the spectral
match between the light and the photoconductive material B. The spectral
response $R(\lambda)$ is given in amperes/watt. The number of signal electrons
released per unit area N_s at the photocathode will be

$$N_s = \int_{\lambda_1}^{\lambda_2} \frac{R(\lambda)E_{fp}(\lambda)}{e} \, d\lambda \text{ signal electrons/m}^2 \quad ,$$

where E_{fp} is the radiant energy received at the focal plane (the photo-
cathode). E_{fp} is related to the radiant intensity of source I_e by
Equation (8), paragraph 4.a. Then,

$$N_s = \frac{R(\Theta)T}{4d^2 e F^2 (m + 1)^2} \int_{\lambda_1}^{\lambda_2} R(\lambda)I_e(\lambda)d\lambda \quad .$$

In paragraph 4.e., $I_e(\lambda) = 4.27$ x the normalized light-source spectrum of
Figure 14. The new value for m is 0.0144. Using the same values for the
remaining terms outside the integral as those used in paragraphs 4.b. and
4.c., we reduce the terms to 9.4×10^{17}. Then,

$$N_s = 9.4 \times 10^{17} \int_{\lambda_1}^{\lambda_2} R(\lambda)I_e(\lambda)d\lambda \quad .$$
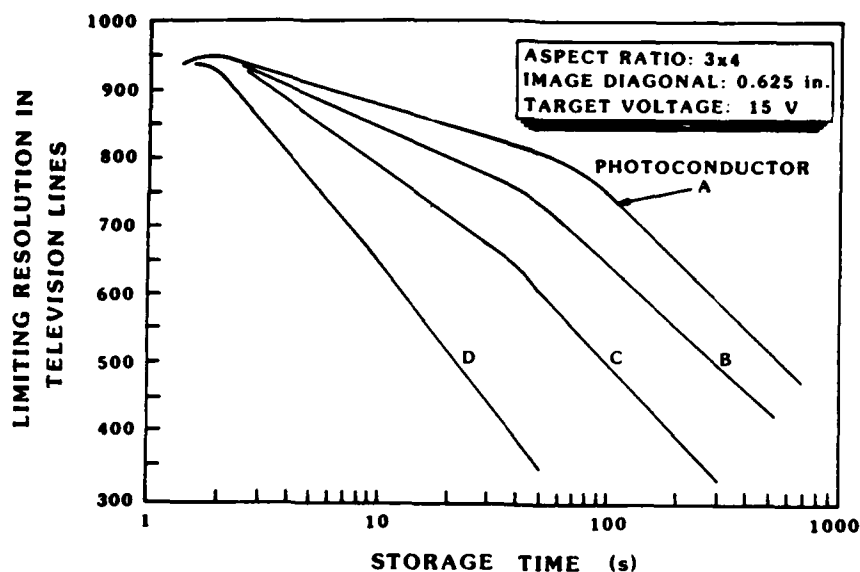
Figure 22. Storage Characteristics of Slow-Scan Vidicons

Between 4000 and 6000 Å, the integral reduces to 4×10^{-2}. Then, $N_s = 3.6 \times 10^{16}$ electrons/m^2, but $n_s = N_s \Delta A$, where ΔA is the minimum picture element area. In the 15.47- by 32-mm raster, there are a maximum of 4215 x 1608 picture elements. Therefore,

$$\Delta A = \frac{15.47 \times 32}{4215 \times 1608} = 7.3 \times 10^{-5} \text{ mm}^2/\text{picture element}$$

or $7.3 \times 10^{-11} \text{ m}^2/\text{picture element}$

and

$n_s = N_s \Delta A = 3.6 \times 10^{16} \times 7.3 \times 10^{-11} = 2.6 \times 10^6$ electrons/ picture element

and the requirement that $S/N = n_s/n_n > 100$ is more then met. The F-stop of the lens can be increased for improved resolution until diffraction limits resolution to less than that desired.

TABLE 3. CHARACTERISTICS OF SLOW-SCAN VIDICONS

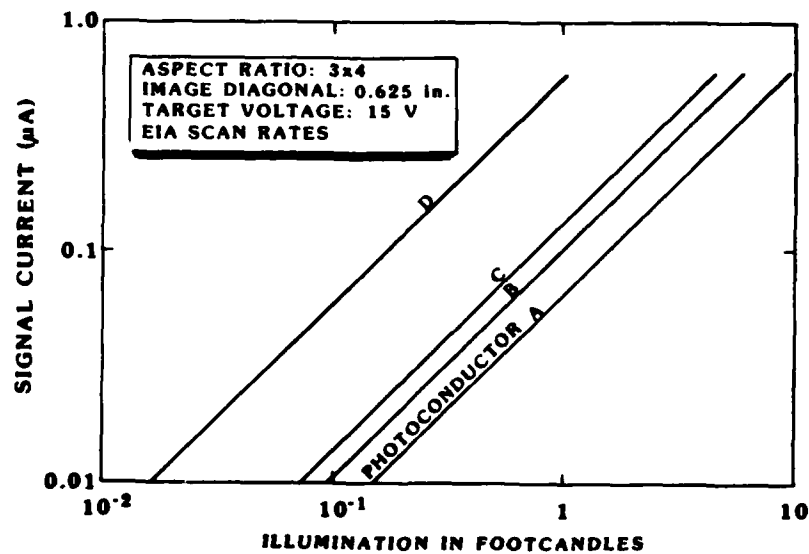| Photoconductor Type	Wavelength of Peak Spectral Response	Sensitivity to White light (2870°K)- Signal Current of a 1" Vidicon at 1 fc at EIA Scan Rates	Storage Characteristics % of Maximum Limiting Resolution Remaining after (beam off)		Dark Current at Room Temperature	Operating Temperature Limits
			10 Sec	100 Sec		
	(nm)	(µA)	%	%	(nA)	°C
A	400	0.065	93	78	0.2	-55° - +45°
B	425	0.11	89	68	0.3	-55° - +60°
C	450	0.13	83	52	0.4	-55° - +60°
D	530	0.6	68	25	1.0	-55° - +60°

Figure 23. Signal Current Transfer Characteristics--EIA Scan Rates.
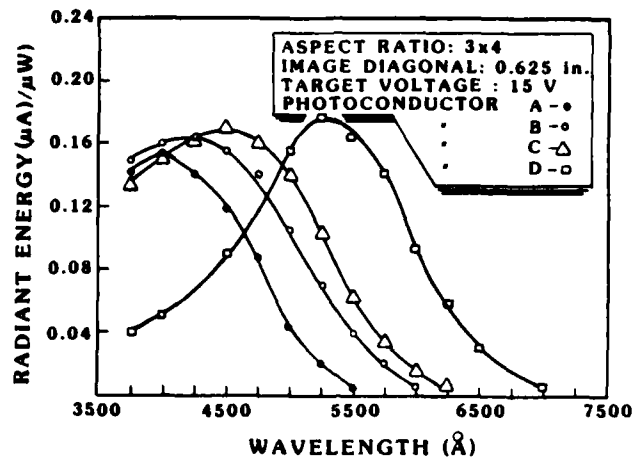
41

Figure 24. Spectral Response of Slow-Scan Vidicons

e. Possible Camera Sources. Table 4 is a fairly comprehensive list of
current EI device manufacturers, which includes current products and products
planned for the future. Note that a NASA/Jet Propulsion Laboratory (JPL)
program is presently developing an 8000 x 8000 element CCD array for a space
telescope application. This will be done by coupling 64 1024 x 1024 element
arrays by means of fiber optics. We have had experience with this technology
from developing a high-speed EI system for an Air Force missile fault analysis
program. We found the fiber optic coupling to be very effective, but it is
expensive.

SECTION III

CONCLUSIONS AND RECOMMENDATIONS

Tests were done to derive the parameters governing operation and resolution of the ARF high-speed camera system. In particular, the system transfer function was found and the spark-gap flash light output was quantized. In addition, our findings were presented in support of the high-speed electronic imaging concept.

The system transfer function includes the camera, camera optics, film, film developing, and effects imposed by the light source, light path, and reflective materials. The transfer function (or MTF) is an industry standard for specifying such systems and gives a concrete definition of the camera system resolution. From the MTF, a 3 percent response point has been calculated as an industry standard reference point. At this point, the minimum object field dimension that can be resolved is 0.7 mm: over the object field of view, the system is capable of resolving a matrix of data points that is 3329 elements high and 1608 elements wide. An EI subsystem must approach this resolution.

Two types of EI devices approach this resolution: an FPS vidicon and a large-target-area slow-scan vidicon. The FPS vidicon can exceed the required resolution, and slow-scan cameras are currently operating at maximum performance at this resolution. The slow-scan camera is more desirable because of linearity considerations.

Considering industry trends is important for this application. Modern solid-state physics is causing a technological revolution in the EI field. Solid-state imaging devices are replacing vacuum tube devices and are allowing smaller size and improved dynamic response and linearity. However, solid state has yet to better the resolution or price of traditional devices. Because solid-state cameras use the same technology as other solid-state devices (integrated circuits, computers, etc.), we expect that performance (resolution) will increase rapidly and price will decrease, and we see evidence of this trend already.

Analysis of the spark-gap flash indicates the spectrum is fairly flat from 400 to 800 nm, which is compatible with most EI devices. The total light output of the unit was also calculated. A survey of the light energy and spectral sensitivity of various EI devices indicates that the light output would probably be sufficient for most devices.

43

TABLE 4. CAMERA SOURCES

Camera	Company	Phone	Contact	Comments
Slow-Scan Video	Sierra Scientific	408-733-6730	William Dyle (Marketing) Paul Mengers (Sales) Harvey Bartholomew (Engineering)	Could have one within 4 mo. with 1608 x 3339 res. and approp. aspect ratio and scan rate
	Westinghouse	607-796-3427	Rolf Myer (Engineering) Pious Nold (Sales)	1608 x 3329 with 1/2-s read-out
FPS Vidicon	Westinghouse			High-resolution 2500 x 2500
Solid State	Fairchild	415-858-6149	Allan King	488 x 380 available. Will call back on advanced developments
	RCA	717-397-7661	Parren Gottshall (Sales)	403 x 512 available, 562 x 512 in 2 years
	Thompson-CSF	201-438-2300	John Mulrow (Sales)	576 x 384 available
	GE Syracuse	315-456-2832 -2808	Dave Hunter	380 x 488 available, 1024 x 1024 in 2-3 years
	Texas Instruments	214-995-2011	Mr. Hoseck	800 x 800 available, 1024 x 1024 now in lab for NASA-JPL (Jim Tamand, 213-354-7734)
	Grumman Aerospace Corp.	714-660-4200	Stan Schwartz (Manager of Engineering)	Stackable linear array on thin-film substrate.

An EI device requires support electronics to control camera functions and temporarily store the image acquired by the EI device. An EI subsystem is composed of the device and the support electronics. At the ARF, each camera would be replaced by an EI subsystem that would be linked to a host computer by means of a single high-speed data link. The host computer collects images from the subsystems for presentation to the operator. Operator interaction coupled with advanced pattern classification techniques is suggested to locate critical projectile points with a consistent accuracy.

Commercial products can be used for the suggested system, but software would need to be generated to provide the necessary functions. Options exist within the EI subsystem for custom-built support electronics that may greatly reduce the costs of upgrading the entire aeroballistics range. The disadvantage of custom electronics is that usually they cannot be maintained by a commercial service organization.

With this report concluding the feasibility study, it becomes clear that EI can be used for high-speed imaging at the aeroballistics range. Economic feasibility is a question that the funding agency must address. Because of the current technological climate, the economics of the project will improve. This advantage must be weighed against the ever increasing cost of maintaining the current facility (caused, for example, by increasing film costs, downtime due to component failures, and unavailability of parts).

The logical continuation of this project is to build a prototype, a state-of-the-art system for high-speed imaging. Building a prototype will allow us to solve problems that may occur in a state-of-the-art design. Thus, EI technology, as applied to high-speed imaging, will be in a state of readiness as applications emerge.

REFERENCES

1. C. A. Spirio, F. Guyker, D. Coy, R. Brown, T. Kuckertz, E. Budge,
    T. Sheheen, and J. Parker, "A Proposal to Perform Electronic Shadowgraph
    Camera Development," Los Alamos National Laboratory proposal DP-F83-10
    (1983).

2. G. L. Winchenbach, D. G. Galanos, and J. S. Kleist, "Description and
    Capabilities of the Aeroballistics Research Facility," Guns, Rockets and
    Explosives Division, Eglin Air Force Base, Air Force Armament Laboratory
    report AFATL-TR-78-41 (February 1978).

3. Electro-Optics Handbook, EOH-11 (RCA Corporation, New York, 1974).

4. J. Johnson, "Analytical Description of Night Vision Devices," in
    "Proceedings of the Seminar on Direct-Viewing Electro-Optical Aids to
    Night Vision," L. Biberman, Ed., Institute for Defense Analyses Study
    S254 (October 1966).

5. Television Engineering Handbook (McGraw-Hill Book Co., New York, 1957),
    pp. 8-22.

6. O. H. Shade, Sr., "Electron Optics and Signal Readout of High Definition
    Return-Beam Vidicon Camera," RCA Rev. 31 (1) (March 1970).

7. C. B. Johnson, "Point-Spread Functions, Line-Spread Functions, and Edge
    Response Functions Associated with MTFS of the Form exp. $[-(w/wc)^n]$,"
    Appl. Opt. 12, 1031 (May 1973).

END

FILMED

1-86

DTIC